

Cite this: *J. Mater. Chem.*, 2012, **22**, 4244

www.rsc.org/materials

Polymer blends with semiconducting nanowires for organic electronics

Sae Byeok Jo,^{†a} Wi Hyoung Lee,^{†a} Longzhen Qiu^{*b} and Kilwon Cho^{*a}

Received 22nd November 2011, Accepted 5th January 2012

DOI: 10.1039/c2jm16059e

This article reviews the recent advances in organic electronics based on polymer blends with one-dimensional (1D) nanowires (NWs) of π -conjugated polymers. Self-assembled polymer semiconducting NWs are fascinating building blocks for their directional extension of inter- and intramolecular π -conjugation. This extensive conjugation provides unique electrical and optical properties that benefit applications in organic electronic devices. Outstanding performances are particularly expected from blending these NWs with insulating polymers or semiconducting molecules. Several representative reports describing NWs prepared from semiconducting/insulating polymer blends, conjugated block copolymers, or electrospinning for use as high-performance organic thin-film transistors (OTFTs) are discussed. The concepts of phase-separation behavior and the growth of crystalline NWs from multi-phase blend solutions are also illustrated. Research into the solubility-induced formation of NWs from semiconducting polymer/n-type small molecule blends for high-efficiency organic photovoltaic solar cells (OPVs) is introduced. In addition, the effects of the chemical properties of conjugated polymers on the optical and electrical properties of NWs and the use of ordered NW structures in OPVs are summarized. This critical review provides insights and a new perspective on the optimization of blend morphologies, which consequently enhances the performance of organic electronic devices.

^aDepartment of Chemical Engineering, Pohang University of Science and Technology, Pohang, 790-784, Korea. E-mail: kwcho@postech.ac.kr

^bKey Lab of Special Display Technology, Ministry of Education, National Engineering Lab of Special Display Technology, National Key Lab of

Advanced Display Technology, Academy of Opto-Electronic, Hefei University of Technology, Hefei, 230009, China. E-mail: lzqiu@ustc.edu

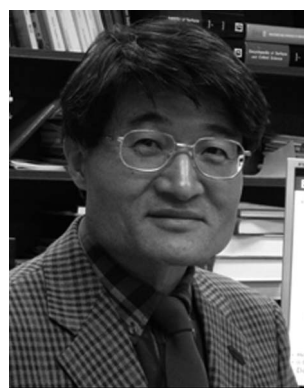
[†] Sae Byeok Jo and Wi Hyoung Lee contributed equally to the work.



Longzhen Qiu

Longzhen Qiu is an associate professor in the Academy of Opto-Electronic at Hefei University of Technology, China. He received B.S. and Ph.D. degrees in chemistry from the University of Science and Technology of China (USTC) in 2001 and 2006, respectively. He was a postdoctoral researcher in Chemical Engineering at Pohang University of Science and Technology (POSTECH), Korea (2006–2008) and in Mechanical & Aerospace Engineering Department at University of California, Los Angeles (UCLA) (2008–2009). From 2009, he joined the faculty at Hefei University of Technology in 2009. His research interests focus on flexible electronics.

From 2009, he joined the faculty at Hefei University of Technology in 2009. His research interests focus on flexible electronics.



Kilwon Cho

Kilwon Cho is a full professor of chemical engineering and director of the Polymer Research Institute at Pohang University of Science and Technology (POSTECH), Korea, and a director of the Global Frontier Research Center for Advanced Soft Electronics. He received his B.S. (1980) and M.S. (1982) from Seoul National University (Korea) in applied chemistry and Ph.D. (1986) from the University of Akron in polymer science. He was a researcher at IBM

Research Center (1987–1988) and then joined the faculty at POSTECH from 1988. His research interests include polymer surface, interface, thin-film and organic electronics. His current research interests are concerned with the development of high-performance organic transistors, organic photovoltaics, and graphene-based electronic devices.

1. Introduction

Considerable progress has been achieved in research directed toward one-dimensional (1D) nanostructures, such as nanowires (NWs), nanofibers, nanorods, nanoribbons, nanobelts, and nanotubes, fabricated from π -conjugated molecules.^{1–3} Many synthetic and post-synthetic routes are available for the fabrication of these organic 1D nanostructures. First, synthetic routes using hard and soft templates are well known among organic synthetic chemists and have been applied toward fabrication of polyaniline and polypyrrole NWs.^{4,5} Although these methods are versatile and can produce 1D polymer nanostructures with control over the shapes, regioregularity and defects are not easy to control, and the incorporation of these nanostructures into functional devices is difficult. Second, synthetic routes using surfactants, such as cetyltrimethylammonium bromide, are desirable methods for synthesizing 1D polymer nanostructures in bulk quantities.^{6,7} However, it is not easy to remove these surfactants after synthesis. Recent articles have reviewed the research front in the area of 1D polymer nanostructure synthesis.

Post-synthetic routes rely on the self-assembly between π -conjugated molecules. π – π Interactions provide the main driving force for the fabrication of 1D organic nanostructures with outstanding optical and electrical properties. Self-assembled 1D structures provide excellent building blocks for active materials in organic electronic devices, such as organic thin-film transistors (OTFTs) and organic photovoltaic solar cells (OPVs). The reader is referred to several well-written review articles describing the fabrication of 1D organic nanostructures from π -conjugated molecules and novel applications of these structures in functional devices.^{1,2,8–11} These review articles mainly treat small-molecule semiconductors with a π -conjugated core, which is indispensable for π – π interactions. However, in the narrow field of 1D polymer nanostructures, little is known about the formation mechanism of polymer semiconducting NWs. Unlike small-molecule semiconductors, the existence of a backbone in the polymer semiconductors inevitably increases the free energy barrier to crystallization. For this reason, it is not easy to fabricate polymer semiconducting NWs with strong π – π conjugation along the growth direction. Rather, the fabricated NWs are believed to consist of crystalline domains and less-organized domains. In spite of these difficulties, polythiophene NWs were first fabricated by Ihn *et al.*¹² and there have been tentative experimental results that synthesized polymer semiconducting NWs from post-synthetic routes. In addition, a review article on thermodynamic and kinetic aspects of polymer crystallization through NWs is available.¹³

Polymer semiconducting NWs fabricated using post-synthetic self-assembly routes are the main theme of this review article. We further focus on the use of polymer blends for the preparation of polymer semiconducting NWs in the active materials of organic electronic devices. For example, common polymers can be added to semiconducting polymers to enhance the electrical performances of OTFTs. Semiconducting polymers can also be blended with other semiconducting molecules to make bulk heterojunction OPVs. We note that previous reports describe the exceptional advantages in fabricating semiconducting polymers in the form of NWs for enhancing the electrical and optical properties of organic electronic devices based on polymer blends.

In this review, we discuss several representative works related to polymer blends with semiconducting NWs and the use of these materials in OTFTs and OPVs. In section 2, the self-assembly methods used to produce polymer semiconducting NWs are briefly reviewed with special attention to the structures and charge transport characteristics of the fabricated NWs. Next, we review reports describing the use of polymer blends with semiconducting NWs in OTFTs (section 3) and OPVs (section 4). Finally, concluding remarks and future research perspectives in these fields are suggested in section 5.

2. Polymer semiconducting NWs

Methods of fabricating polymer semiconducting NWs using post-synthetic self-assembly routes can be grouped into three categories: 1) solution-phase self-assembly, 2) external force-driven self-assembly, and 3) template-assisted self-assembly. These categories may not cover all existing self-assembly methods; however, they are useful from the perspective of considering the driving forces for self-assembly. Solution-phase self-assembly uses the characteristics of π – π interactions between conjugated backbones, whereas conjugated polymers are present in the solution state without application of external forces or spatial constraints. As the solubility of a conjugated polymer in solution decreases, the polymer begins to precipitate and form ordered aggregates by interchain π – π stacking of the conjugated polymers.¹⁴ The addition of a nonsolvent into the solution or decreasing the solution temperature are well-known methods for decreasing the solubility and activating the formation of ordered aggregates.^{15–20} Although an increase in the conjugation length through π – π stacking is commonly observed from analysis of the absorption spectra, the exact structure of the ordered aggregates is the subject of considerable debate. However, it is believed that some folded conformations of the conjugated polymers are favored in solution.^{14,17} By solution-casting the ordered precursors onto a substrate, 1D polymer NWs can typically be obtained. An interesting property of NW growth is that NWs can only grow at appropriate solvent evaporation rates and at certain concentrations.^{17,20–22} In addition to self-assembly from the solution phase, post-deposition treatments, such as thermal annealing or solvent vapor annealing, are widely used for the growth of NWs, and these techniques have received considerable attention because of the simplicity of the associated processes.^{21,23}

Fig. 1 shows a TEM image and stacking scheme of typical poly(3-hexylthiophene) (P3HT) NWs. Because π – π interactions provide the main driving force for the 1D growth of conjugated polymers, the growth direction coincides with the π – π stacking direction in NWs grown by solution-phase self-assembly. In addition, alkyl side chains are oriented normal to the substrate surface to minimize the surface energy. This structure also minimizes the unfavorable interactions between the conjugated backbone and the solvent and is widely accepted as the general structure of P3HT NWs.^{12,13,21,24,25}

Fig. 1, lower panel, schematically shows three types of charge-transport pathways in P3HT NW networks, including interchain, intrachain, and inter-grain transport. Interchain and intrachain charge transport are considered to be the two main pathways for charge transport in conjugated polymers, and they

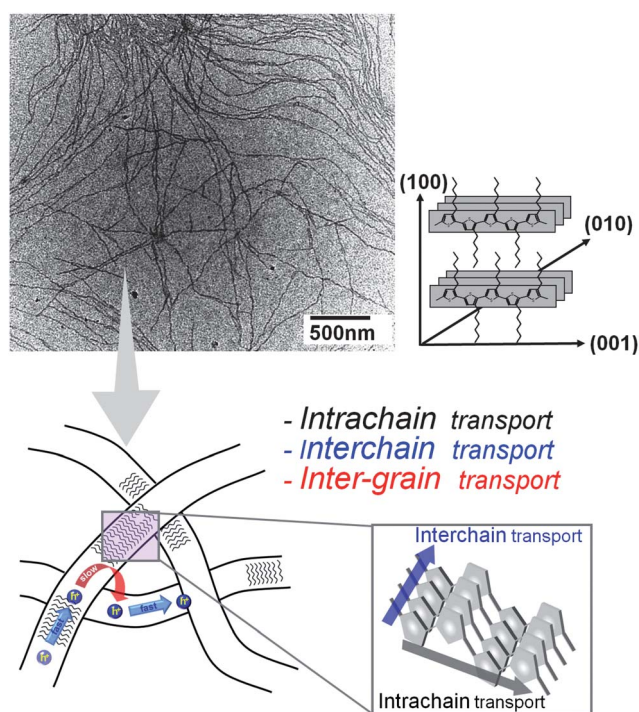


Fig. 1 TEM images of poly(3-hexylthiophene) (P3HT) NWs and the chemical structure of P3HT along the molecular axis (upper panel). Charge transport characteristics of P3HT NWs in the molecular stacking scheme (lower panel).

facilitate two-dimensional charge transport in a direction substantially parallel to the substrate surface.²⁶ On the other hand, grain boundaries and defects are detrimental to charge transport because charge carriers scatter at these sites. The NW dimensions are important parameters for achieving utility in functional devices. The molecular weight and regioregularity of P3HT, as well as the concentration of P3HT and the preparation conditions, can alter the width and height of the NWs.^{27,28} Other components blended with P3HT can also affect the crystallization characteristics of P3HT to produce P3HT NWs of different dimensions. As with carbon nanotubes (CNTs),²⁹ long NWs with few defects and grain boundaries are usually preferred as active materials in OTFTs. Furthermore, these NWs provide good vertical pathways for charge transport, which strongly indicates that 1D NWs with high aspect ratios can be useful building blocks for vertical-type devices, such as OPVs.^{30–32} Another merit of the long NWs lies in their low percolation threshold and excellent mechanical properties. If the dimensions of the NWs are fixed, good electrical properties may be obtained by reducing the number of junctions. To this end, aligning NWs along one direction is highly recommended in OTFTs in which charge carrier transport proceeds along a parallel direction.^{33,34} However, NWs fabricated by solution phase self-assembly are randomly organized in most cases because external forces that could align the NWs are absent.

External force-driven self-assembly and template-assisted self-assembly can convey alignment on the NWs. Shear forces applied to polymer solutions or to solid pallets can induce directional crystallization of conjugated polymers.^{35,36} However, P3HT does not easily crystallize into NWs using these methods.

The short alkyl chains in P3HT are too short to crystallize into well-ordered structures, possibly due to the liquid-like characteristics of these alkyl chains.³⁷ On the other hand, conjugated polymers having a high crystallinity, such as a poly(2,5-bis(3-alkylthiophen-2-yl)thieno[3,2-*b*]thiophene) (PBTTT)–cyclopentadithiophenebenzothiadiazole (CDT-BTZ) copolymer can be crystallized into NWs under application of external forces.^{38,39} Furthermore, high-directionality NWs could be fabricated by dip-coating using highly crystalline conjugated polymers.³⁹ In polymer semiconducting NW structures fabricated by external force-driven self-assembly, the main chains usually aligned along the direction of an applied force, resulting in the formation of NWs with strong anisotropy.⁴⁰ This result contrasts with the self-assembly scheme shown in Fig. 1 and suggests that NW structures can vary with the characteristics of the conjugated polymers and the fabrication procedures. Electrospinning can also produce NWs with various diameters, morphologies, and compositions.⁴¹ However, it is not easy to control the nanoscale ordering within polymer semiconducting NWs during electrospinning. For this reason, little data is available on the molecular structures of electrospun NWs. The difficulty may be that conjugated polymers display low crystallinity compared to common polymers with high crystallinity, such as nylon or polyethyleneoxide. Common polymers with highly ordered polymer chains have been used in electrospinning processes for NW fabrication.^{42,43} The difficulties in producing polymer semiconducting NWs will be discussed in section 3.3 in more detail.

Template-assisted self-assembly uses templates into which conjugated polymers may be crystallized. One common approach is to introduce a template with regular holes of nanoscale diameter. Conjugated polymers may be sucked into these nanoholes and form NWs or nanotubes by crystallizing within the confined geometry. For example, polyfluorene NWs and nanotubes were synthesized using a porous anodic aluminum oxide (AAO) membrane, yielding alignment of the main chains along the long axis of the nanoholes.^{44,45} Furthermore, interesting optical properties, such as optical microcavity behavior, were reported using these NWs.⁴⁶ Because the vertically aligned NW arrays with defined dimensions could easily be obtained using this method, the fabricated NW arrays were useful as building blocks in ordered bulk heterojunction solar cells.^{47,48} In addition to periodically patterned templates, other templates are also available for inducing directional crystallization among conjugated polymers. For example, highly ordered pyrolytic graphite (HOPG) was used as a template for P3HT or poly(3,3'-didodecylquaterthiophene) (PQT-12) crystallization in a certain molecular ordering.^{49,50} Because strong π – π interactions provided a key force for aligning the conjugated polymers, lying-down structures were usually obtained *via* interactions between the conjugated backbones and the HOPG. Similarly, graphene, which is a single sheet of graphite, can serve as a uniform and versatile template for the growth of conjugated polymers because monolayer graphene is free from step-edges or kinks, which prohibit the highly ordered growth of conjugated polymers on HOPG.^{51,52} 1,3,5-Trichlorobenzene (TCB) can also be used as a template for epitaxial P3HT growth. The stacking periodicity of TCB molecules coincides with the repeating periodicity of P3HT and, thus, highly crystalline P3HT NWs can form on TCB.^{53,54} New methods for NW fabrication and the synthesis of

new conjugated polymers greatly increase the potential utility of polymer semiconducting NWs in the active materials of organic electronic devices. In sections 3 and 4, we will focus on how these polymer semiconducting NWs can be blended with other components for use in OTFTs and OPVs.

3. OTFTs based on polymer blends with semiconducting NWs

Thin-film transistors (TFTs) are a type of field effect transistor that is widely applied in flat panel displays, radio frequency identification (RFID) tags, or sensing devices. A TFT consists of one semiconductor layer, one dielectric layer, and three electrodes (source, drain, and gate). Despite the success of Si-based TFTs, there is great interest in TFTs prepared using organic semiconductors as the active layer (OTFT) due to their suitability for fabricating lightweight, flexible, low-cost, large-area electronic devices. In particular, soluble polymer semiconductors enable fast and cost-effective manufacturing of electronic devices using established printing technologies. A general approach to obtaining the properties required for practical applications has been to design and synthesize new materials. Over the past decade, a variety of small-molecule semiconductors, such as pentacene, metal phthalocyanines, or perylenetetracarboxyldiimide, and conjugated polymers, such as regioregular P3HT, PBTTT, PQT-12, and CDT-BTZ, have been developed to achieve OTFT devices with high performances.

Blends of conjugated polymers present an alternative and facile way to tune and optimize the electronic properties of devices because the blends take advantage of the properties of each material, and can result in material performances that exceed those of the individual components. For example, ambipolar field effect charge transport has been reported in binary blends of p-type and n-type conjugated polymers or oligomers.^{55–57} However, the inherent inhomogeneity and disordering in the polymer blends tend to disturb charge transport.⁵⁸ The phase separation characteristics of the blends significantly affect the electric and optoelectronic properties. Recently, the integration of polymer blends with semiconducting NWs was shown to be beneficial for achieving high performances in TFT devices. In general, three types of semiconductor–NW/insulating polymer composites have been used in OTFTs.

3.1. Semiconducting/insulating polymer blends with embedded semiconducting NWs

Semiconducting and insulating polymer blends have attracted increasing interest because they can combine the electronic properties of semiconducting polymers with the low-cost fabrication and excellent mechanical characteristics of the insulating polymers. However, the presence of an insulating component usually hinders charge transport. Monotonic degradation of the electronic performance with increasing insulating polymer content has been observed for OTFT devices with semiconducting/insulating polymer blends as the active material.^{58,59} Forming self-stratified structures *via* vertical phase separation in polymer blend thin films presents an effective approach to maintaining the connectivity of the semiconducting layers in the channel region between the source and drain electrodes.^{59–64}

However, phase separation in polymer blends is very complicated, and the final morphology in a blend film is highly sensitive to many factors (such as the solvent evaporation rate, the solubility parameters, the film–substrate interactions, the surface tension of each component, and the film thickness). Thus, vertical phase separation can only occur under extreme conditions. Lateral phase separation is more common than vertical phase separation because the forces that contribute to the formation of lateral structures minimize the interfacial area.^{65,66}

The percolation threshold depends strongly on the aspect ratio. One-dimensional nanostructures, such as NWs, nanotubes, and nanoribbons, geometrically favor the preservation of connectivity at low contents. CNTs provide a good example of such properties. Electrical percolation at a content as low as 0.03 wt% can be achieved in polymer composites with well-dispersed single-walled carbon nanotubes (SWCNTs).⁶⁷ Due to their rigid π -conjugated backbones, polymer semiconductors, especially poly(3-alkylthiophene)s (P3ATs), can often crystallize into 1D nanostructures in dilute solutions under conditions of limited solubility (see section 2). Polymer blends comprising NWs can be easily achieved by dissolving the materials in a common solvent, followed by additional processing steps.

In 1993, Ihn and coworkers first demonstrated the preparation of P3AT NWs from a poor solvent.¹² Based on this result, Lu *et al.*⁶⁸ reported preparation of semiconducting/insulating polymer blends with embedded NWs. Typically, a dilute poly(3-butylthiophene) P3BT solution (10 mg mL⁻¹) was prepared in a poor solvent, *o*-dichlorobenzene (ODCB), at elevated temperatures. Because of the limited solubility of P3BT in ODCB at room temperature, cooling of the prepared hot P3BT/ODCB solution gradually induced self-assembly of the P3BT chains into NWs. These NWs had widths of 15 nm, lengths exceeding 10 μ m, and aspect ratios (L/d) larger than 670. Upon addition of PS to a suspension of P3BT NWs, followed by deposition of the mixed solution *via* spin coating, P3BT/PS composite films with interconnected P3BT NW networks within the PS matrix were obtained. The conductivity of the P3BT–NW/PS composite film was enhanced nearly an order of magnitude relative to that of pure P3BT. Conductive atomic force microscopy (C-AFM) imaging revealed that the activation energy for charge transport within the P3BT NWs was reduced upon formation of an extremely large interfacial area between the conjugated polymer and the insulating polymer matrix, which contributed to a high carrier mobility.⁶⁹

Cho and coworkers⁷⁰ extended the use of semiconducting/insulating polymer blends with embedded NWs to OTFT devices. The system employed was a blend of P3HT with PS. The blends obtained from chloroform showed typical spinodal decomposition morphologies with poor P3HT crystallinity. As a result, the electronic performance degraded monotonically with increasing PS content. In stark contrast, the blend films obtained from a marginal solvent, methylene chloride (CH₂Cl₂), yielded a network of super-long highly crystalline P3HT nanofibers embedded in an insulating PS matrix (Fig. 2). The use of this material as an active layer in TFT devices yielded an electronic performance comparable to that observed from pristine P3HT in blends comprising P3HT and amorphous PS at P3HT contents as low as 5 wt%. This structure thus provided good encapsulation of the active P3HT nanofibers and, therefore, significantly

improved the environmental stability of the devices. In addition, this simple, mild and reproducible method is suitable for the fabrication of large-area flexible electronic devices.

Recent results demonstrated that the morphology and electronic properties of P3HT NWs depend both on the solubility in the solvent and on the aging time of the precursor solution.^{20,71} The results obtained from a mixed solvent containing chloroform (CF), which is a common solvent for both P3HT and PS, and dioxane (DI), which is a good solvent for PS but a poor solvent for P3HT, demonstrated a sigmoidal relationship between the probability of forming P3HT NWs and the DI/CF ratio or the aging time. Under optimized conditions, devices based on P3HT/PS blend films containing only 1 wt% P3HT showed field effect mobilities as high as $1 \times 10^{-2} \text{ cm}^2 \text{ V}^{-1} \text{ s}^{-1}$, comparable to that obtained from pristine P3HT films.

Ink-jet printing is an attractive direct patterning technique for the cost-effective fabrication of organic electronic devices

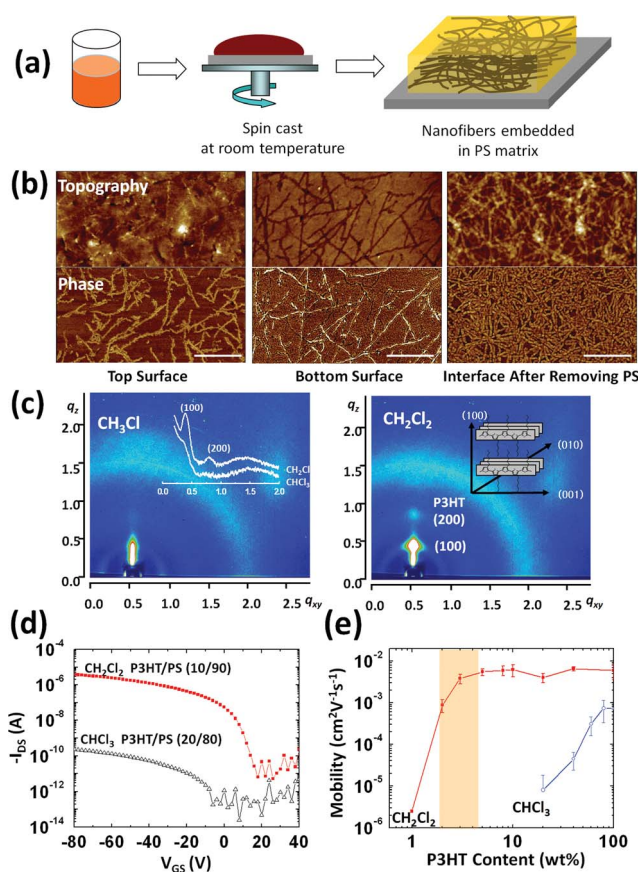


Fig. 2 (a) Schematic representation of the formation of a nanofibrillar network in a PS matrix. (b) AFM topography (top) and phase (bottom) images of P3HT/PS (5/95) blend films spin-cast from CH_2Cl_2 ; top surface (left), bottom surface (middle), and interface after selectively dissolving PS (right). The scale bar indicates 500 nm. (c) 2D grazing incidence angle X-ray diffraction (GIXRD) of P3HT/PS (10/90) films spin-cast from CHCl_3 (left) or CH_2Cl_2 (right) solutions. The inset represents 1D out-of-plane X-ray profiles extracted from the 2D patterns. (d) Typical transfer characteristics of the devices based on P3HT/PS (10/90) blends from a CH_2Cl_2 solution and P3HT/PS (20/80) blends from a CHCl_3 solution. (e) Average field effect mobility measured in the saturation region as a function of the P3HT content in the blends. (Reproduced with permission from ref. 70. Copyright Wiley-VCH Verlag GmbH.)

because designed patterns of an ink material can be directly deposited onto a substrate without the use of a pre-patterned mask or additional etching processes.^{10,72–74} However, the performance of electronic devices based on inkjet-printed organic semiconductors is lower than that of devices fabricated by spin-casting or vapor deposition processes, due to the uneven morphology and random orientations of the crystalline structures in printed organic semiconducting layers.⁷⁵ Cho and coworkers⁷⁵ demonstrated inkjet printing of P3HT/PS blends with semiconducting NWs from a mixed solvent composed of chlorobenzene (CB) and cyclohexanone (CHN) (80 : 20 v/v ratio) (Fig. 3). The inkjet-printed blend films having this unique structure provided effective pathways for charge carrier transport through semiconductor NWs with significantly improved environmental stability. Moreover, printed single-droplet transistors yielded a high ratio of the field effect mobility to the bulk conductivity, thereby dramatically increasing the on/off characteristics.

The production of electronic circuits based on organic devices crucially depends on organic semiconductors patterned at the micrometre scale. The technique of choice in the inorganic electronics microelectronics industry has been photolithography. However, patterning of organic semiconductors *via* photolithography is challenging because organic semiconductors tend to degrade upon exposure to light⁷⁶ and the chemicals used in photolithography may have detrimental effects on organic thin films.⁷⁷ A blend of organic semiconductors and photocrosslinkable insulating polymers was photolithographically

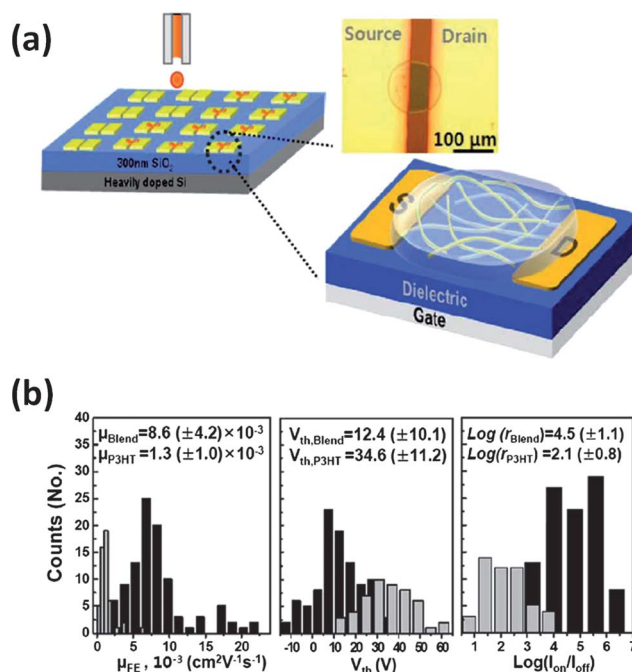


Fig. 3 (a) Schematic diagram of the fabrication process and optical microscopy image of an inkjet-printed single-droplet transistor based on a P3HT/PS blend. P3HT/PS blend films printed from a CB/CHN mixed solvent show unique structures, with P3HT NWs dispersed in a PS matrix. (b) Summary of the device characteristics for 100 transistors based on P3HT NW/PS (20 : 80) blends (black) and 50 transistors based on P3HT, printed from CB (gray) in different batches. (Reproduced with permission from ref. 75. Copyright Wiley-VCH Verlag GmbH.)

patterned to form OTFTs (Fig. 4).⁷⁸ The semiconducting polymer of the blend, P3HT, was present as a nanofibrillar network and displayed excellent electronic properties. The insulating polymer matrix, poly(vinyl cinnamate) (PVCn), provided the photosensitivity required for photopatterning. By dividing the functions of charge transport and photoreactivity into P3HT and PVCn, respectively, perturbations in the conjugation of the backbone due to crosslinking were effectively eliminated. Furthermore, the blends were crosslinked *via* a photodimerization reaction of cinnamate without using an initiator, which avoided the trapping effects arising from photoinitiators. As a consequence, the photopatterned TFT devices showed large on/off ratios ($>10^5$) and high mobilities ($0.015 \text{ cm}^2 \text{ V}^{-1} \text{ s}^{-1}$) comparable to those of devices patterned by conventional means using the same semiconducting materials.

3.2. NWs from conjugated block copolymers

Conjugated block copolymers are promising molecular building blocks because they can self-assemble into any of several nanoscale morphologies. Copolymers containing a polythiophene and insulating flexible segments can self-assemble into NWs from solution. McCullough and coworkers⁷⁹ synthesized diblock and triblock copolymers composed of P3HT and PS segments with different block compositions. These conjugated copolymers self-assembled into well-defined NWs with 30–40 nm widths upon solvent evaporation. Recently, Yu *et al.*⁸⁰ reported that P3HT-*b*-PS with 85 wt% P3HT displayed significantly enhanced charge transport properties and environmental stability compared to the P3HT homopolymer, with up to a factor of 2 increase in the mobility ($0.08 \text{ cm}^2 \text{ V}^{-1} \text{ s}^{-1}$). Diblock copolymers of P3HT and poly(methyl acrylate) (PMA) were also synthesized and formed nanofibrillar structures, as shown in Fig. 5(a). OTFTs based on P3HT-*b*-PMA exhibited good charge carrier mobilities approaching that of pure P3HT.⁸¹

Crystalline–crystalline diblock copolymers of P3HT and PE (P3HT-*b*-PE) were prepared and exhibited crystallization-induced phase segregation behavior, during which the P3HT

blocks were predominantly expelled to the surfaces of cast films where they formed highly ordered fibrillar structures upon solvent evaporation above the melt temperature of PE, as shown in Fig. 5(b).⁸² Field effect transistors based on these nanofibrillar structures showed saturated charge carrier mobilities as high as $2 \times 10^{-2} \text{ cm}^2 \text{ V}^{-1} \text{ s}^{-1}$ and on/off current ratios of $\sim 10^5$, even at 90 wt% insulating polyethylene. In addition, the P3HT-*b*-PE diblock copolymers displayed outstanding flexibility and toughness with elongations at break exceeding 600% and a true tensile strength of around 70 MPa. This material opened a path toward robust and truly flexible electronic components.

Jenekhe and coworkers⁸³ recently demonstrated that block copoly(3-alkylthiophene)s composed of side-chains of several sizes, *e.g.*, poly(3-hexylthiophene)-*b*-poly(3-cyclohexylthiophene) (P3HT-*b*-P3cHT), could be self-assembled into NWs. Interestingly, the morphology could be tuned by varying the block composition. Field effect transistors fabricated from P3HT-*b*-P3cHT thin films showed a field effect mobility of $0.0019 \text{ cm}^2 \text{ V}^{-1} \text{ s}^{-1}$, independent of thermal annealing.

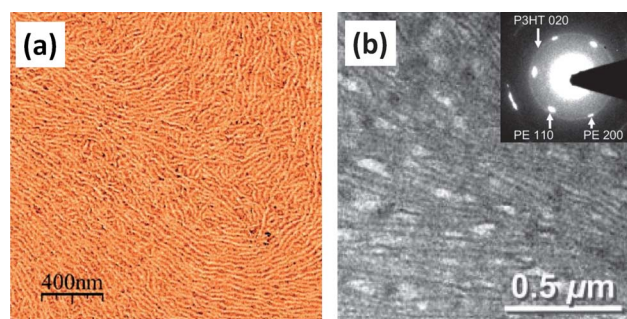


Fig. 5 (a) AFM phase images of rr-P3HT-*b*-PMA (43–57) on SiO₂ treated with OTS-8. (b) Transmission electron micrograph of P3HT-*b*-PE (35–65) processed at elevated temperatures under conditions in which the P3HT moiety crystallized first. The inset represents the corresponding electron diffraction pattern. (Reproduced with permission from ref. 81 and ref. 82. Copyright Wiley-VCH Verlag GmbH.)

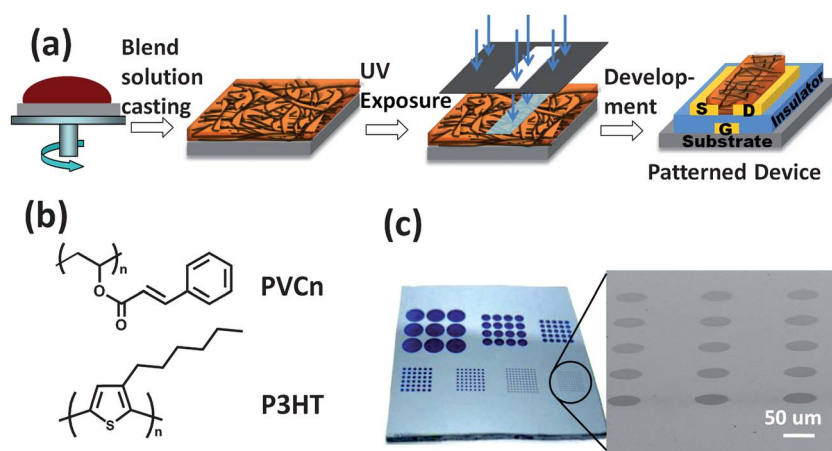


Fig. 4 (a) Schematic illustration of the photolithographic patterning process. (b) Chemical structures of P3HT and poly(vinyl cinnamate) (PVCn). (c) Photographic and SEM images of photopatterned P3HT/PVCn (10/90 w/w) blend films. (Reproduced with permission from ref. 78. Copyright The Royal Society of Chemistry.)

3.3. Electrospun NWs from conjugated polymer blends

Electrospinning is a simple, inexpensive, and scalable method for producing long continuous nanofibers of diverse materials under a high electric field. Electrospun nanofibers are of great interest because they allow various materials to be combined into nanofibers with a range of dimensions. Electrospun nanofibers can exhibit novel properties and phenomena as a result of the intermolecular interactions, confinement effects, and extended chain conformation. Babel *et al.* found that electrospun nanofibers of binary blends of poly[2-methoxy-5-(2-ethylhexoxy)-1,4-phenylenevinylene] (MEH-PPV) with P3HT phase-separated into smaller domains than in the spin-coated thin films, resulting in significant energy transfer.⁸⁴ In contrast, energy transfer was absent in electrospun nanofibers of MEH-PPV blends with poly(9,9-dioctylfluorene) (PFO), possibly due to the large scale of the phase separation in the nanofibers. Nanofibers of MEH-PPV/P3HT blend nonwoven mats exhibited p-channel transistor characteristics with hole mobilities in the range of $(0.05\text{--}1) \times 10^{-4} \text{ cm}^2 \text{ V}^{-1} \text{ s}^{-1}$, and the hole mobility increased by an order of magnitude after correcting for the channel area.

Electrospinning of low molecular weight rigid chain conjugated polymers with limited solubility is not as easy as electrospinning of conventional insulating polymers. Therefore, insulating polymers are often added to assist in the electrospinning of conjugated polymers. A blend of doped polyaniline (PANI) and poly(ethylene oxide) (PEO) was electrospun into nanofibers with diameters in the range 120–300 nm.⁸⁵ Bottom-gate transistors from the PANI/PEO nanofibers exhibited field effect characteristics at low source–drain voltages with hole mobility of $1.4 \times 10^{-4} \text{ cm}^2 \text{ V}^{-1} \text{ s}^{-1}$. Field effect transistor based on electrospun nanofibers of pure P3HT were reported by Craighead⁸⁶ and Pinto.⁸⁷ However, the morphology of the P3HT nanofibers was poor, and many beads were present along the fibers. Insulating polymers, such as PEO,⁸⁸ poly(ϵ -caprolactone) (PCL),^{89,90} PS and PMMA,⁹¹ have been widely used as carrier polymers to improve electrospinning. The field effect mobilities of electrospun nanofibers of pure P3HT were in the range of $0.017\text{--}0.192 \text{ cm}^2 \text{ V}^{-1} \text{ s}^{-1}$. Electrospun P3HT/polymer blend nanofibers also showed field effect behavior with mobilities of $1.6 \times 10^{-5}\text{--}2 \times 10^{-3} \text{ cm}^2 \text{ V}^{-1} \text{ s}^{-1}$, which were lower than those of electrospun pure P3HT nanofibers. On the other hand, a high mobility of $2 \text{ cm}^2 \text{ V}^{-1} \text{ s}^{-1}$ and an on/off current ratio of 10^5 were reported for an OTFT based on P3HT/PCL blend nanofibers, with replacement of a traditional silicon oxide gate dielectric with a polyelectrolyte gate dielectric (Fig. 6).⁹⁰

4. OPVs based on polymer blends with semiconducting NWs

Over the past few decades, OPVs have attracted much attention due to the low costs of fabrication, the feasibility of high-throughput production, and the wide applicability to environmentally friendly energy sources.^{92,93} Recently, the power-conversion efficiencies (PCEs) of OPVs have increased beyond 8% through development of new materials and device architectures using advanced processing techniques,^{94–97} which is approaching the threshold for commercial viability.⁹⁸ The most frequently accessed materials in the field of OPVs are the p-type

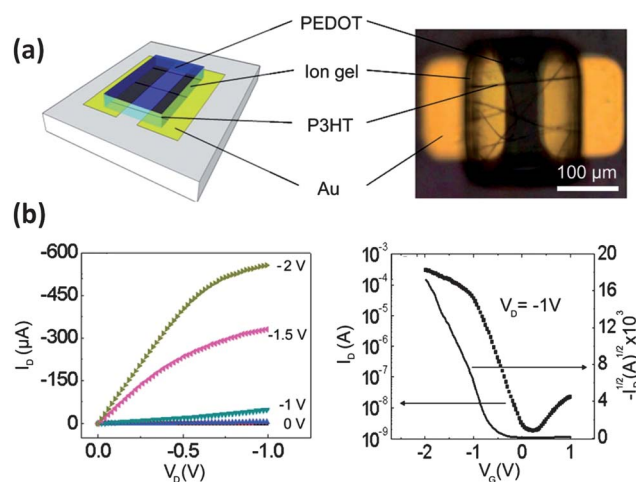


Fig. 6 (a) Schematic diagram and optical microscopy image showing an ion-gel gated transistor formed from P3HT NWs. (b) The output and transfer characteristics of the arrayed transistor. (Reprinted with permission from ref. 90. Copyright 2010 American Chemical Society.)

polymers, such as P3HT, and narrow band-gap co-polymers containing both electron donating and withdrawing moieties, such as poly[2,6-(4,4-bis(2-ethylhexyl)-4H-cyclopenta[2,1-*b*:3,4-*b'*]-dithiophene)-*alt*-4,7-(2,1,3-benzothiadiazole)] (PCPDTBT).^{99,100} [6,6]-Phenyl-C₆₁-butyric acid methyl ester (PC₆₁BM) and C₆₀-indene bis-adduct (ICBA) are also promising materials for use in n-type materials.^{101,102}

Certain device architectures have yielded optimal photovoltaic performances using randomly distributed p/n junctions in the donor–acceptor blends, called bulk heterojunctions (BHJs). Control over phase separation and the formation of crystalline structures can critically determine the photovoltaic performances of OPV devices, with optimal results obtained from highly efficient exciton separation and charge transport.¹⁰³ Because the pathway for charge transport is required to be developed under the electric fields perpendicular to the electrodes, some degree of vertical and lateral phase separation in the otherwise well-mixed blend films is required to ensure a charge transport pathway to each electrode (Fig. 7(b)).¹⁰⁴ Moreover, with several compelling reports, it is widely believed that the transport and collection of holes and electrons can differ depending on the carrier mobilities, where the accumulation of one type of carrier can limit the saturation current by forming a non-zero equilibrium space charge. However, the intrinsic mobilities of conventional donors and acceptors, such as P3HT and PCBM, display significantly imbalanced ratios without any post-treatment.¹⁰⁵

There are several processing techniques such as annealing^{31,106–108} or solvent mixing^{109,110} to achieve optimal morphology and balanced charge transport through self-assembly of the polymers during spontaneous phase separation. The different solubility window of the donor and acceptor molecules in solution produces blend morphologies that are not equilibrated (Fig. 7(a)).¹¹¹ Thermal energy or solvent vapors permits the molecules in a blend film to spontaneously rearrange to achieve a more stable conformation. However, since the extent of the formation of crystalline structures competes with the degree of phase separation, the precise control over the development of

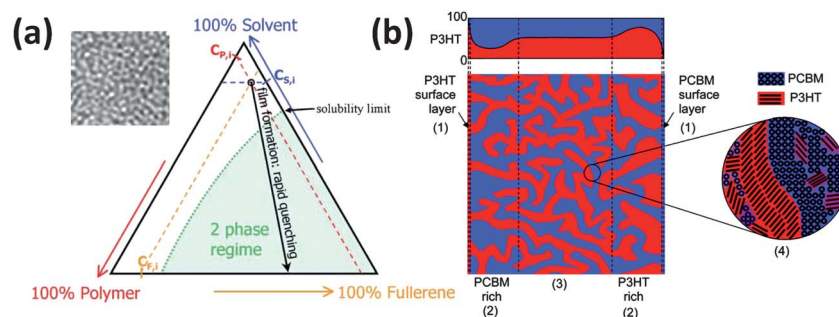


Fig. 7 (a) Schematic phase diagram of a 3-phase polymer–fullerene–solvent system at constant temperature and pressure. The arrows indicate the direction of increasing concentration whereas the green envelope indicates the solubility limits for phase separation. (b) Schematic diagram of the phase separation and crystal formation in a P3HT:PCBM blend film. (Reproduced with permission from ref. 111 and ref. 104. Copyright 2011 American Chemical Society and Royal Society of Chemistry.)

crystalline structure is an important issue for the further enhancement of the photovoltaic performances.

As mentioned in the previous sections, the crystalline structures, such as 1D NWs, significantly enhance the charge carrier mobility, providing efficient charge transport pathways. In this sense, the incorporation of 1D crystalline structures, especially the semiconductor NWs, with its directional charge transport with an enhanced charge carrier mobility, provides an efficient means for optimizing and enhancing the photogeneration of charge carriers.^{30,32,112,113} Studies of the development or introduction of 1D NWs in blend films *via* post-synthetic methods are critical for the development of NW based OPV devices. The formation of 1D NWs within blend systems is complicated by the presence of other phases, such as solvents or small molecules; therefore, the kinetic and thermodynamic mechanisms underlying the formation of 1D NWs in multi-phase systems require thorough investigations.

In this section, we discuss the strategies for the use of self-assembled semiconductor NWs in the multi-phase blend films toward development of high-performance OPVs. The mechanisms underlying the nanostructure formation in a blend will be reviewed, and recent results concerning the incorporation of NWs using fractional precipitation and selective solubility methods will be introduced. We also present the effects of the chemical structure on the formation of NWs and the resulting photovoltaic performance. Finally, the fabrication of ordered NW structures using nanotemplates for high-performance OPVs will be briefly covered. This critical review provides insights and a new perspective into optimizing the morphologies of photoactive layers and enhancing the photovoltaic performances of OPVs.

4.1 Formation of NWs in multi-phase blend systems

The crystallization and phase behavior of donor–acceptor blend systems may be understood by analyzing the thermodynamic properties of a blend system. Fig. 8(b) shows the thermodynamic phase diagram of a representative P3HT/PCBM blend system.^{114,115} The glass transition temperature of the blend depended strongly on the PCBM content. As the PCBM content increased, the T_g of the P3HT decreased, indicating the limits of intermolecular interactions in the presence of a second

component. Hot melt blends comprising P3HT and PCBM in a 1 : 1 blend ratio yielded two phases upon cooling: the L + S_{PCBM} phases, with prior solidification of the PCBM. Further down to 150 °C, recrystallization of the blend film occurs at transition temperatures that varied depending on the PCBM content. As the PCBM content increased, the transition temperature decreased. This behavior indicated that heat treatment of the blend film lent mobility to both the P3HT chains and the PCBM; therefore, recrystallization of the P3HT molecules was hampered by the presence of a second component. The crystallization of P3HT molecules prior to crystallization of the second component was, therefore, critical for the development of nanostructures, such as NWs.

Another report described the bimolecular crystallization of donor polymers and PCBM based on the intercalation of PCBM between the side chains of the polymer molecules. In this case, the hole mobility decreased significantly upon intercalation of the PCBM molecules.^{116,117} The bimolecular crystallization depended on the density of the side chains, *i.e.*, the relative sizes of the side chain spacings and the PCBM derivatives. P3HT, with short chain spacings, did not yield co-crystallization, which was advantageous for introducing the NWs into the blend (Fig. 8(a)). The topographic images and photocurrent generation of the blend films¹¹³ (Fig. 8(c)) showed a clear distinction between the NWs and the rest of the amorphous blend materials. Interestingly, the careful selection of a solvent with selective solubility or the addition of PCBM before or after NW formation did not affect the final film morphology. This behavior will be discussed briefly at the end of this section and in greater detail in section 4.3.

In addition to the development of crystalline structures, phase separation between the two components during film formation and subsequent annealing can affect film morphology and, therefore, device performance. During annealing, the low miscibility of a polymer and a small molecule can induce profound vertical and lateral phase separation due to the entropy reduction associated with mixing.¹¹⁸ During solvent vapor annealing, solvent molecules penetrate into the blend films to provide the same effects as are obtained from thermal annealing.³¹ Thermal energy or the presence of solvent molecules provide components with a freedom to move to the most stable conformations, and concentration fluctuations in the vertical and

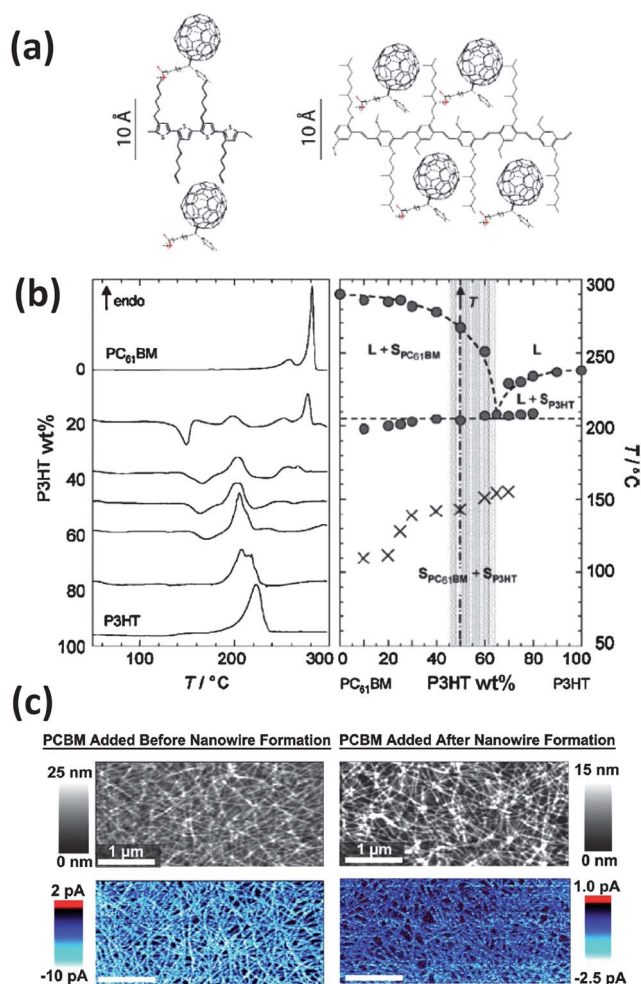


Fig. 8 (a) Schematic diagram of fullerene intercalation between polymer side chains. (b) The phase behavior of the P3HT/PCBM blend system. The DSC thermogram (left) shows the variations in the glass transition temperature as a function of PCBM composition. The crosses in the phase diagram (right) represent the onset of recrystallization as a function of PCBM content. (c) The topography and photocurrent AFM images under short circuit conditions for the P3HT wires formed before (right) and after (left) PCBM addition. (Reproduced with permission from ref. 115, ref. 117 and ref. 113. Copyright Wiley-VCH Verlag GmBH and 2011 American Chemical Society.)

lateral directions are observed to increase with the annealing time.¹¹⁹ As mentioned previously, crystallization through strong interchain interactions can further expel a second component, inducing more severe phase separation. The miscibility of the two components,¹²⁰ the annealing time, and the temperature (or solvent) can determine the concentration fluctuations in the vertical or lateral directions, which critically affects the final film morphology.

The ability to separately control the phase separation and crystallization processes during annealing would be beneficial for improving the properties of crystalline NWs. This may be possible through the judicious use of the three-component system phase diagram, which includes the two blend components and the solvent (Fig. 7(a)). During film formation, the miscibility of each molecule in the solvent critically affects the initial

morphology of a blend film. As the solvent evaporates, the concentration of each component increases and eventually passes through its solubility limit. Depending on the composition and miscibility of each component in the solvent, the blend can simultaneously phase-separate into multiple phases, including a homo phase of the PCBM, a homo phase of the amorphous P3HT, a homo phase of the crystalline P3HT and an interfacial mixture of the P3HT and PCBM. Selection of the solvent and processing conditions can be used to control the phase separation, *i.e.*, the sequential formation of each phase, so that the independent incorporation of NWs into the blend film is possible without the unavoidable coarsening during phase separation in an annealing process.

To achieve fine control over the blend morphology, several fabrication methods have been developed, such as the incorporation preformed P3HT NW.^{30,32,112} The interactions between the solvent and each component can affect the phase separation and the resulting film morphology and microstructure. The selective solubility of the solvent, namely, the high solubility of P3HT and the low solubility of PCBM, or *vice versa*, provides conditions similar to those present during annealing, whereas the second component remains soluble or precipitates earlier than the first. In the remaining part of this section, recent approaches to the efficient incorporation of NWs, with optimization of the morphology, will be discussed.

4.2. Solubility-induced formation of NWs within a blend

The crystallization of conjugated polymers, especially P3HT, has been extensively studied due to its versatile variations in the chain conformations and the solid-state packing. As previously discussed, the selective development of crystalline NWs in a blend was achieved by controlling the solubility of the blend solution. P3HTs display thermochromic and solvatochromic behaviors, which can be detected as changes in the light absorption as a function of temperature or solvent solubility as a result of changes in the chain conformations. The changes in the chain conformations in a solvent can be utilized to prepare NWs in solution, and the most common approach is the fractional precipitation method. In marginal solvents for P3HTs, such as xylene, cyclohexanone, methylene chloride, dioxane, and hexane, P3HT molecules tend to fold themselves into helical conformations, thereby forming nanoscale fibrillar structures.^{14,121,122} The solubility of P3HT chains in a marginal solvent can increase at elevated temperatures above the saturation concentration at room temperature. During careful cooling at a controlled cooling rate, the P3HT molecules can form aggregates that self-assemble into NWs over aging time (Fig. 9(a)). Control over the solvent power by mixing solvent provides similar results as are achieved from fractional precipitation methods.³² The solubility-induced selective crystallization of P3HT can proceed by i) the fractional precipitation method, ii) the solvent mixing method, or iii) solvent annealing. The first two methods mainly deal with the formation of NWs in the solution phase, and the latter concerns the treatment of blend films. Several other methods with unconventional approaches are available as well, such as ultrasonic-assisted self-assembly.¹²³

Berson *et al.* first introduced P3HT nanofibers into OPV devices.¹¹² The nanofibers of P3HT were formed in *p*-xylene by

a fractional precipitation method, then they were separated from the amorphous phase. The self-assembled NWs showed a red shift and the evolution of a shoulder near 550 nm in the UV-Vis absorption spectrum, as well as the clear development of an ordered crystalline structure in the (100) direction (Fig. 9(b), (c)).¹⁷ The purified nanofibers were then redispersed in the same solvent with the PCBM. The photovoltaic performance of a blend film containing 75 wt% P3HT nanofibers with 25 wt% amorphous phase clearly showed an enhanced PCE of up to 3.6%. Despite the superior electrical and optical properties of P3HT nanofibers, the amorphous phase must be present to some extent to sufficiently interact with the acceptor molecules.

To avoid the difficulties associated with fabricating NWs separately from the blend, nanofibers may be fabricated within a blend by introducing a selective solvent and by employing the fractional precipitation and solvent mixing methods. Kim *et al.* reported the use of a marginal solvent for P3HT, methylene chloride (MC).³⁰ MC provided limited solubility for the P3HTs at room temperature, while maintaining a relatively high solubility for the second component, PCBM. At higher temperatures, near the boiling point of MC, P3HT dissolved to yield a reddish-yellow color. As the temperature decreased, the P3HT began to

solidify and the solution turned purple. The formation of NWs was clear based on the UV-Vis spectra (Fig. 9(b)). As the aging time of the solution increased, an absorption band at $\lambda = 450$ nm, which was characteristic of amorphous P3HT chains, gradually disappeared, and the characteristic absorption peaks of crystalline P3HT near $\lambda = 550$ nm and 600 nm were more pronounced. The absorption spectrum of PCBM (335 nm) remained unchanged as the solution aged. The morphology of the P3HT NWs and their blends with PCBM provided clear evidence for the selective development of P3HT NWs without interference from the second component (Fig. 9(d), (e)). The photovoltaic performances of the P3HT NW:PCBM blends showed enhanced photocurrent generation with increasing aging time, reaching PCEs up to 4%. These enhancements were explained in terms of the improved balance between the hole and electron mobilities as the crystallinity of P3HT increased. Moreover, the NW-incorporated devices exhibited charge transfer rates approaching unity, indicating the efficient charge extraction (Fig. 10(a)). In addition, the maximum photocurrent in the saturation regime increased, indicating an increase in the exciton generation rate caused by enhanced photon absorption with a longer conjugation length in the P3HT NWs.

Another promising approach includes the mixing of good and marginal solvents to control the solvent properties.³² Cyclohexanone is a marginal solvent for P3HT. The addition of cyclohexanone to a 33 vol% concentration to the P3HT:PCBM solution in chlorobenzene induced crystallization of the P3HTs. The XRD and UV-Vis absorption spectra clearly showed the increase in P3HT crystallinity upon addition of cyclohexanone. Subsequent thermal annealing of the blend films increased the aggregation of PCBM without damaging the P3HT NWs. The photovoltaic performance also showed an improved balance between the hole and electron mobilities. Interestingly, the optimum thickness of the blend film almost doubled upon incorporation of the P3HT NWs into the blend (Fig. 10(b)). As discussed in the previous sections, the optimum thickness of the photoactive layer was determined by the interplay between the charge transport characteristics and the optical absorption. This result suggested that the NWs provided enhanced charge transport by increasing the hole mobility so that additional charge carriers provided by the thicker active layers could be collected at the electrode.

Control over the kinetic aspects of film formation using mixed solvents has proven to be useful for obtaining optimized morphologies with enhanced crystallinity.^{19,31,100,109,124,125} Non-reactive chemical additives, such as 1,8-alkanedithiol, diiodoalkane, or *N*-methyl-2-pyrrolidone, have two major characteristics: i) a high boiling point, or ii) selective solubility for the P3HT and PCBM. A schematic diagram of the process is shown in Fig. 11(a). During film formation in the presence of small amounts (<5 vol%) of chemical additives, the main solvent, usually a good solvent for both P3HT and PCBM, evaporates first leaving a high-boiling-point additive in the blend film. The remaining additives are usually good solvents for the PCBM but poor solvents for the P3HT. As in the fractional precipitation methods using a marginal solvent, the additive induces aggregation of P3HT, leaving the PCBM phase mobile. Prolonged spinodal decomposition using the additive results in coarse vertical and lateral phase separation. However, unlike thermal

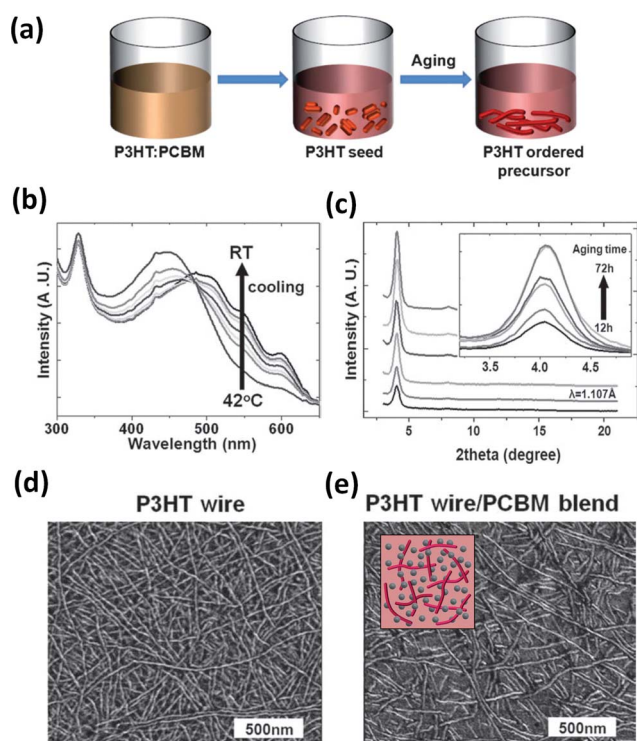


Fig. 9 (a) Schematic diagram showing NW growth in the P3HT:PCBM blend solution using the fractional precipitation method. (b) The UV-Vis absorption spectra of the P3HT NW:PCBM blend films as a function of the aging time. As aging proceeded, clear vibronic features at $\lambda = 550$ nm appeared. (c) The XRD pattern obtained from the blend films as a function of aging time. The topographic images of (d) the homo P3HT NW and (e) the P3HT NW:PCBM blend. (Reproduced with permission from ref. 32 and ref. 30. Copyright Royal Society of Chemistry and Wiley-VCH Verlag GmbH.)

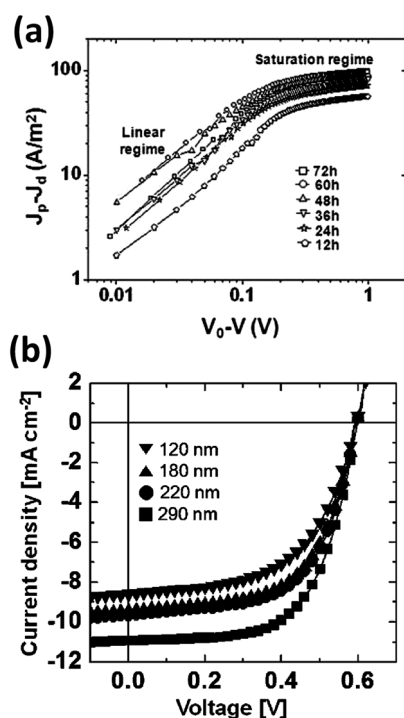


Fig. 10 (a) The experimental photocurrent as a function of the effective bias voltage for the P3HT NWs as a function of aging time. V_0 represents the compensation voltage at which the photocurrent reached zero. (b) Current–voltage curves for the P3HT NW:PCBM devices as a function of thickness. The optimum thickness of the device was almost double that of devices without NWs. (Reproduced with permission from ref.32 and ref.30. Copyright Royal Society of Chemistry and Wiley-VCH Verlag GmbH.)

annealing, the formation of P3HT NWs is not affected by the presence of a second component, and the crystalline NWs developed properly (Fig. 11(b)). The photovoltaic performances of the devices prepared using the additives showed remarkably enhanced PCEs in the P3HT:PCBM blend systems (Fig. 11(c)). These additive approaches are also effective in the preparation of amorphous systems because they induce phase separation *via* selective solubility. Several other approaches, such as ultrasonic-assisted self-assembly of P3HT,¹²³ are effective for the fabrication of blend solutions containing P3HT NWs.

The incorporation of NWs into a blend solution containing the active materials or during film formation is effective for optimizing the morphologies of OPV devices. The fractional precipitation method or solvent mixing using a marginal solvent have successfully incorporated NWs into blend solutions. Additives can enhance the formation of NWs during film formation. The resultant device performances yield balanced electron and hole mobilities and a high charge collection efficiency. Further applications and generalizations of these techniques have required more profound investigations into the formation of NWs and their effects on the photovoltaic performance. The importance of the chemical structure, molecular weight (MW), regioregularity (RR), and polydispersity indices (PDI) on device performance has also been investigated. In the following section, the chemical aspects of NW blends will be discussed.

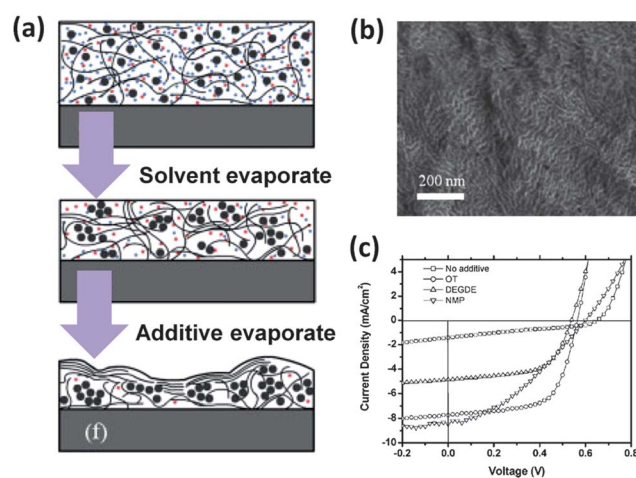


Fig. 11 (a) Proposed model for film formation during the drying process. The black wire corresponds to the P3HT chains, black dots correspond to PCBM, and the red and blue dots represent the 1,8 octanedithiol and dichlorobenzene molecules, respectively. (b) The morphology of the P3HT:PCBM blend film prepared in the presence of chemical additives. An aggregated fibrillar structure was observed to be dominant. (c) The current–voltage characteristics as a result of processing with various chemical additives. (Reproduced with permission from ref.109, Copyright Wiley-VCH Verlag GmbH.)

4.3. Effects of the chemical properties on the characteristics of NWs for OPVs

The chemical structure of a polymer determines the interchain interactions and the resultant thermodynamic behaviors. The lengths of the side chains,^{122,126,127} molecular weights,^{128,129} and regioregularity^{130,131} affect the self-assembly of poly(alkylthiophene)s (P3AT).

First, the effects of the alkyl side chain length on the crystallization of P3ATs have been investigated, along with the thermodynamic, optical, and morphological properties. Despite the fact that shorter alkyl side chains increase the propensity for self-assembly among polymer backbones, P3HT, with a hexyl side group, was found to provide the highest photovoltaic performance with conventional film formation and processing techniques.¹²⁶ However, the NW incorporated OPV devices with other than hexyl side-chain have showed compelling results.^{121,122} Several researchers investigated the photovoltaic performance of P3AT with a variety of side chain lengths, from 4 (butyl) to 12 (dodecyl). TEM images of the morphologies of the P3AT films with different side chain lengths clearly indicated development of NWs in the blends containing PCBM (Fig. 12(b)). XRD studies clearly indicated the formation of ordered crystalline structures with *d*-spacings that increased with increasing side chain length in the (100) direction. The increased *d*-spacings between the conjugated backbones with longer side chains reduced interchain charge transport. The space charge limited (SCL) mobility also showed a reduced hole mobility with increasing side chain length, which was analogous to the field effect mobility trends for the P3ATs.¹³² The melting temperature of the P3AT decreased linearly with increasing side chain length¹²⁷ (Fig. 12(c)). This trend was explained in terms of the increased entropy of the longer P3AT side chains.¹²⁷ In a blend of P3AT and PCBM, the

longer side chains facilitated the diffusion of PCBM, resulting in a higher degree of lateral phase separation with dimensions of a few hundreds of nanometres.¹²⁷ The morphology obtained in the presence of the long side chains indicated formation of spherical P3HT crystalline domains rather than nanofibrillar structures. Despite the enhanced interchain charge transport along the direction of the NWs (the (010) axis) formed with shorter side chains, a pronounced imbalance between the electron and hole mobilities restricted the photovoltaic performance. A reduced fill factor (FF) clearly demonstrated the effects of the mobility imbalance. The open circuit voltage (V_{OC}), on the other hand, decreased with decreasing side chain length due to the

up-shift of HOMO level in the P3ATs with shorter side chain lengths.

The optical properties of P3AT NWs included an increase in the absorption spectrum as the side chain length increased, with pronounced vibronic features at $\lambda = 610$ nm and 520 nm (Fig. 12(d)). This behavior could be understood in terms of the interchain coupling due to H-aggregate chromophores in the P3AT NWs. Generally, the first transition (0–0) in an H-aggregate is symmetry-forbidden, although it is weakly allowed in the presence of disorder induced by the individual polymer chains. As interchain coupling with the excitons increased, the 0–0 transition was further suppressed with longer side chains.¹³³

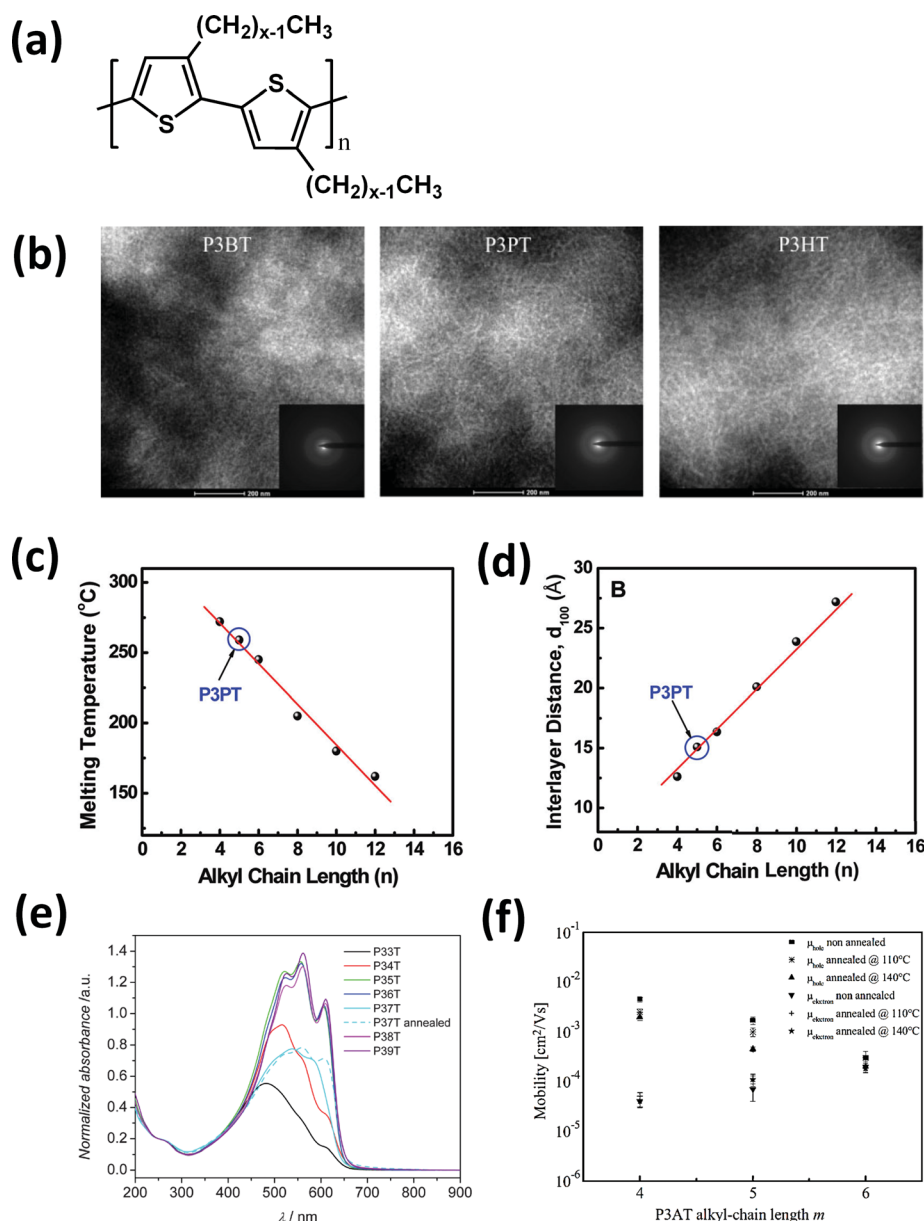


Fig. 12 (a) Chemical structure of P3AT, (b) TEM image of the P3AT:PCBM morphology. The solubility-induced formation of NWs was clearly observed in all cases. (c) The melting point and (d) interlayer distance as a function of alkyl chain length. (e) UV-Vis absorption spectra for the P3AT/PCBM blend. (f) The space charge limited hole and electron mobilities as a function of the alkyl chain length. The effects of thermal treatment are also presented. (Reproduced with permission from ref. 122, ref. 126, and ref. 133. Copyright 2009 American Chemical Society, Wiley-VCH Verlag GmbH and Royal Society of Chemistry.)

The increased interchain distance decreased the interchain coupling so that the transition increased, as shown in Fig. 12(c). Control over the optical and electrical properties of NWs in OPV devices should be considered systematically to achieve optimal device performance.¹²⁶

The MW and RR of P3AT significantly affected the performance of OPV devices. The development of NW structures with a high RR is obviously advantageous for enhancing the optical and electrical properties; however, severe phase separation in the film can result by favoring aggregation of PCBM.¹³⁰ Several reports have examined the effects of the MW of P3HT on device performance and have shown that higher MWs provide a higher hole mobility, although lower MW P3HT produces finer crystalline structures.^{122,131} These effects are still under debate because several factors, such as interchain/intrachain charge transport and chemical defects in the chain ends, may be in competition. Studies of the photovoltaic performance also report that the coexistence of highly crystalline NWs and low-crystalline regions in a blend film is important.¹²⁹

The excellent electrical and optical properties of NWs have inspired other approaches to applying NWs in OPVs. The following section discusses ordered arrays of NW structures for use in OPV devices.

4.4. Ordered NW structures for use in OPVs

Ordered BHJ structures have been studied using a variety of methods to directly utilize the large interfacial areas between donors and acceptors with the spontaneous development of charge transport pathways to the electrodes.^{134,135} Unlike conventional BHJ structures, periodic arrays of nanopillars or nanopores composed of donors (or acceptors) can provide large interfacial areas for exciton separation and charge transfer without the isolation of separated charge carriers. To this end, researchers have worked toward reducing domain sizes below hundreds of nanometres, which corresponds to the dimensions of the exciton diffusion length. Several soft imprinting templates, such as AAO or block copolymers, have been developed for direct incorporation into the formation of solution-phase semiconducting NWs including organic, inorganic semiconductors such as ZnO and GaAs^{136,137} and quantum dots such as CdS and CdSe.^{136,138} Template-free growth of aligned organic and inorganic nanopillars using hydrothermal methods¹³⁹ or unconventional thermal deposition methods^{140–142} for the application of organic or hybrid solar cells have also been reported.

Among these methods, nanoscale hexagonal arrays of AAO with controllable pore dimensions have yielded successful results with enhanced photovoltaic performances. Kim *et al.* utilized an AAO template to construct nanopillar P3HT structures.¹³⁴ The patterned template was 150 nm in height, 50 nm in width, and 100 nm in pore-to-pore distance (Fig. 13(b)). A hot melt of P3HT in contact with an AAO template filled the pores by capillary force under vacuum conditions. The molecular ordering in P3HT nanopillars was also investigated. XRD studies showed the face-on (010) alignment of P3HT chains in the nanopillar structure, which is advantageous for interchain charge transport (Fig. 13(c)). This result is explained by the nano-confinement effect that affects molecular ordering of P3HT.¹⁴³ Conducting AFM images indicated a 10-fold increase in the conductivity of

the nanopillar structure compared to the film. To fabricate the ordered BHJ structures, fullerene was deposited onto the P3HT nanopillar structures by thermal evaporation. The PCE of the nanopillar-based OPVs increased by a factor of 7 compared to the planar structure. The photoluminescence (PL) spectrum, shown in Fig. 13(d), displayed remarkable quenching in the blend film with the P3HT nanopillar structures, indicating that the large interfacial area reduced exciton loss from radiative recombination. Li *et al.* fabricated n-type nanorods using a crosslinkable fullerene derivative in the presence of an AAO template.¹³⁵ The [6,6]-phenyl-C₆₁-butyric styryl dendron ester (PCBSD) film on the AAO template with dimensions similar to those described above was pressed to produce nanostructures (Fig. 13(e)). PCBSD was then crosslinked at high temperatures, and the AAO was subsequently removed. Since the crosslinked nanostructure was robust to solution processes, the P3HT:ICBA blend was solution-cast on top of the nanostructure. The device showed remarkable PCEs up to 7.3% with a high FF of 72%. The reduced recombination loss from the guaranteed charge pathways and enhanced charge generation from the enlarged interfacial areas resulted in high-performance OPV devices. The stability of the devices improved due to the robustness of nanostructured bottom layer.

Nanofibers of P3HT:PCBM blend have also been fabricated with AAO templates (Fig. 14(e), (f)).¹⁴⁴ The PL spectra show the quenching of 0–0 and 0–1 transition peaks, indicating efficient charge transfer from P3HT to PCBM. A single nanowire was separated and its photovoltaic performance was measured with different compositions. Due to the poor development of the morphology, the PCE of the devices was under 1%. However, as previously reported micron-scale fiber OPVs,¹⁴⁵ the nanofiber OPV gives an insight into a new architecture for potential flexible power sources in the future. More direct utilizations of aligned nanofiber structures in OPV devices have been reported. Briseno *et al.* grafted P3HT chains on template-free grown ZnO NWs by functionalization of the end-group in P3HT (Fig. 14(a)–(d)).¹³⁶ The P3HT chains spontaneously form ordered domains at the interface with ZnO NWs. An isolated single ZnO/P3HT nanowire with Al and Au electrodes showed effective generation of photocurrent. Due to the low photovoltaic performance of nanofiber based OPVs, further investigation of the structures and properties inside the nanofibers needs to be carried out. In conclusion, the control over the ordered 1-D nanostructures in OPVs could provide not only a platform for examining the effects of nanostructuring, but also significant improvements in the performance of BHJ-based OPVs. Moreover, detailed analysis of the nanostructures inside the blend films would lead to the development of a viable candidate for flexible power sources.

5. Conclusions and outlook

Polymer blends containing semiconducting NWs are promising active materials for organic electronic devices, such as OTFTs and OPVs. The semiconducting NWs with π -conjugated molecules face-to-face self-assembled along the π - π stacking direction provide high charge-carrier mobility along the long axis of the NW. Blending offers an effective approach to tune the properties of organic semiconductors and meet practical applications by combining the advantageous properties of each

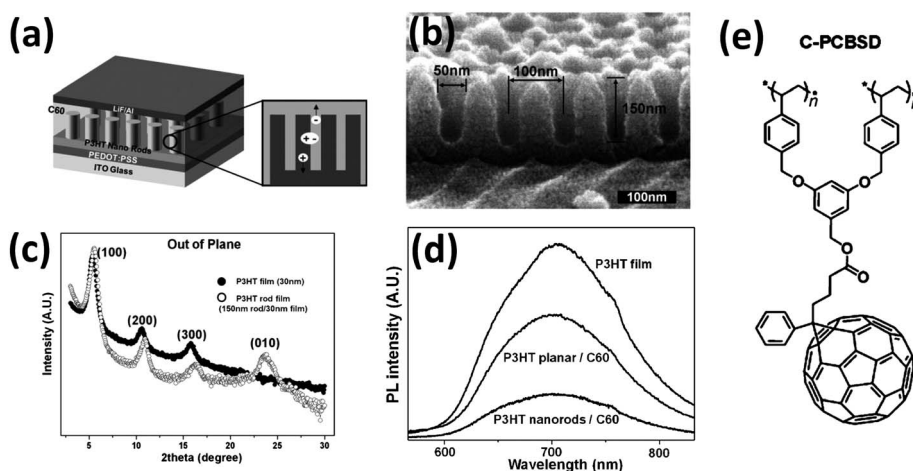


Fig. 13 (a) Schematic diagram of P3HT nanorod-based ordered BJJ solar cells. Photoinduced charge transfer (PICT) occurred at the interface between the P3HT and C₆₀. (b) FE-SEM image of the AAO template with controlled pore size. (c) The out-of-plane grazing incidence XRD intensities for P3HT nanorods and films. The peaks indicate the face-on orientations (010) of the P3HT chains in the nanorods. (d) The photoluminescence spectra of a P3HT single layer and solar cells constructed with deposition of C₆₀ on top of the P3HT nanorods. (e) The molecular structure of the cross-linkable fullerene derivative used in the n-type nanorod formation. (Reproduced with permission from ref. 134 and ref. 135. Copyright Wiley-VCH Verlag GmBH.)

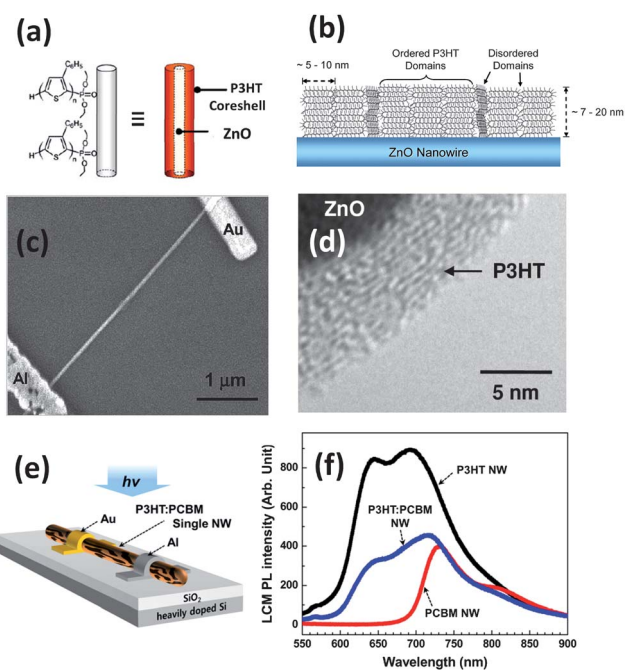


Fig. 14 Schematic representation of (a) P3HT grafted ZnO NWs and (b) the ordering of P3HT lamellae at the interface with ZnO nanowires. (c) SEM image of single nanowire devices and (d) TEM image of the interface between ZnO and aligned P3HT. (e) Schematic illustrations of the nanodevice with Au and Al electrodes using a P3HT:PCBM single NW fabricated through a wetting method by using an AAO template. (f) PL spectra for the single NWs of P3HT, PCBM and P3HT:PCBM composite. (Reproduced with permission from ref. 136 and ref. 144. Copyright Wiley-VCH Verlag GmBH and Elsevier.)

component. The use of these materials in OTFTs has significantly improved several device properties, including the material costs for fabrication, the device performances, the mechanical properties, the environmental stability, and the device

patterning. However, several fundamental and technological challenges remain before practical applications may be commercially implemented. Firstly, although it has been observed that the OTFTs based on semiconducting NWs/insulating polymer blends showed a mobility comparable to that based on pristine semiconductors at very low NW content, the reason for this phenomenon remains unclear. It is well known that charge transport in OTFTs based on pristine semiconductors only takes place in the first few molecular layers near the gate dielectric layer. When the semiconductor content in blends is decreased, the NW density at the dielectric–semiconductor interface will be reduced accordingly. Therefore, charge transport in blends and the effects of the polymer matrix on charge transport must be studied in greater depth to resolve the charge transport mechanism. Secondly, NWs in present polymer blends are randomly oriented. It will be extremely beneficial for improvement of OTFT performance if the NWs are aligned in a direction parallel to the charge carrier transport. Finally, new polymer matrix-bearing semiconducting NWs must be developed to achieve novel properties and/or to provide new functionalities.

The introduction of NWs into the blend layers of OPV devices provides a promising approach to optimizing photovoltaic performance. Directional hole transport with a balance in the carrier mobilities can significantly enhance photocurrent generation. However, independent control over the two most critical factors, NW formation and phase separation, remains a challenge in this field. There is still room for further improving vertical and lateral phase separation by incorporating NWs, thereby enhancing the performances of OPV devices. Furthermore, it is critically important to understand the role of NWs in the photoactive layers with respect not only to charge transport, but also to the optical, thermal, mechanical, and process engineering aspects of device preparation and performance. Furthermore, thorough investigation of the nanostructure formation in the confined environment should be carried out for

the enhancement of device performances and future application of flexible electronics. With the continuous emergence of new materials and NWs, the development of new blend materials and the investigation of the chemical, physical, and environmental fundamentals of the behavior of NWs in the blend will provide a new area in optimization of organic electronics devices for future printed electronics.

Acknowledgements

This work was supported by a grant (Code No. 2011-0031627) from the Center for Advanced Soft Electronics under the Global Frontier Research Program of the Ministry of Education, Science and Technology, Korea, and the Major State Basic Research Development Program of China (2010CB334704), the National Natural Science Foundation of China (61040015, 21174036, 51103034), the Research Fund for the Doctoral Program of Higher Education of China (20100111120006), the Anhui Province Natural Science Foundation (11040606M146).

References

- 1 F. S. Kim, G. Q. Ren and S. A. Jenekhe, *Chem. Mater.*, 2011, **23**, 682.
- 2 A. L. Briseno, S. C. B. Mannsfeld, S. A. Jenekhe, Z. Bao and Y. N. Xia, *Mater. Today*, 2008, **11**, 38.
- 3 A. N. Aleshin, *Adv. Mater.*, 2006, **18**, 17.
- 4 H. D. Tran, D. Li and R. B. Kaner, *Adv. Mater.*, 2009, **21**, 1487.
- 5 D. Li, J. X. Huang and R. B. Kaner, *Acc. Chem. Res.*, 2009, **42**, 135.
- 6 X. T. Zhang, J. Zhang, Z. F. Liu and C. Robinson, *Chem. Commun.*, 2004, 1852.
- 7 A. M. Wu, H. Kolla and S. K. Manohar, *Macromolecules*, 2005, **38**, 7873.
- 8 G. De Luca, W. Pisula, D. Credgington, E. Treossi, O. Fenwick, G. M. Lazzerini, R. Dabirian, E. Orgiu, A. Liscio, V. Palermo, K. Mullen, F. Cacialli and P. Samori, *Adv. Funct. Mater.*, 2011, **21**, 1279.
- 9 S. H. Liu, W. C. M. Wang, A. L. Briseno, S. C. E. Mannsfeld and Z. N. Bao, *Adv. Mater.*, 2009, **21**, 1217.
- 10 J. A. Lim, H. S. Lee, W. H. Lee and K. Cho, *Adv. Funct. Mater.*, 2009, **19**, 1515.
- 11 W. Pisula, M. Zorn, J. Y. Chang, K. Mullen and R. Zentel, *Macromol. Rapid Commun.*, 2009, **30**, 1179.
- 12 K. J. Ihn, J. Moulton and P. Smith, *J. Polym. Sci., Part B: Polym. Phys.*, 1993, **31**, 735.
- 13 J. A. Lim, F. Liu, S. Ferdous, M. Muthukumar and A. L. Briseno, *Mater. Today*, 2010, **13**, 14.
- 14 N. Kiriy, E. Jahne, H. J. Adler, M. Schneider, A. Kiriy, G. Gorodyska, S. Minko, D. Jehnichen, P. Simon, A. A. Fokin and M. Stamm, *Nano Lett.*, 2003, **3**, 707.
- 15 S. D. D. V. Rughooputh, S. Hotta, A. J. Heeger and F. Wudl, *J. Polym. Sci., Part B: Polym. Phys.*, 1987, **25**, 1071.
- 16 K. Yoshino, P. Love, M. Onoda and R. I. Sugimoto, *Jpn. J. Appl. Phys.*, 1988, **27**, L2388.
- 17 Y. D. Park, H. S. Lee, Y. J. Choi, D. Kwak, J. H. Cho, S. Lee and K. Cho, *Adv. Funct. Mater.*, 2009, **19**, 1200.
- 18 K. Zhao, L. J. Xue, J. G. Liu, X. Gao, S. P. Wu, Y. C. Han and Y. H. Geng, *Langmuir*, 2010, **26**, 471.
- 19 Y. D. Park, J. K. Park, J. H. Seo, J. D. Yuen, W. H. Lee, K. Cho and G. C. Bazan, *Adv. Energy Mater.*, 2011, **1**, 63.
- 20 Y. D. Park, S. G. Lee, H. S. Lee, D. Kwak, D. H. Lee and K. Cho, *J. Mater. Chem.*, 2011, **21**, 2338.
- 21 D. H. Kim, Y. D. Park, Y. Jang, S. Kim and K. Cho, *Macromol. Rapid Commun.*, 2005, **26**, 834.
- 22 D. H. Kim, Y. Jang, Y. D. Park and K. Cho, *J. Phys. Chem. B*, 2006, **110**, 15763.
- 23 G. H. Lu, L. G. Li and X. N. Yang, *Adv. Mater.*, 2007, **19**, 3594.
- 24 J. A. Merlo and C. D. Frisbie, *J. Polym. Sci., Part B: Polym. Phys.*, 2003, **41**, 2674.
- 25 J. A. Merlo and C. D. Frisbie, *J. Phys. Chem. B*, 2004, **108**, 19169.
- 26 H. Sirringhaus, P. J. Brown, R. H. Friend, M. M. Nielsen, K. Bechgaard, B. M. W. Langeveld-Voss, A. J. H. Spiering, R. A. J. Janssen, E. W. Meijer, P. Herwig and D. M. de Leeuw, *Nature*, 1999, **401**, 685.
- 27 J. H. Liu, M. Arif, J. H. Zou, S. I. Khondaker and L. Zhai, *Macromolecules*, 2009, **42**, 9390.
- 28 T. Shimomura, T. Takahashi, Y. Ichimura, S. Nakagawa, K. Noguchi, S. Heike and T. Hashizume, *Phys. Rev. B: Condens. Matter Mater. Phys.*, 2011, **83**, 115314.
- 29 T. Sekitani, H. Nakajima, H. Maeda, T. Fukushima, T. Aida, K. Hata and T. Someya, *Nat. Mater.*, 2009, **8**, 494.
- 30 J. S. Kim, J. H. Lee, J. H. Park, C. Shim, M. Sim and K. Cho, *Adv. Funct. Mater.*, 2011, **21**, 480.
- 31 J. H. Park, J. S. Kim, J. H. Lee, W. H. Lee and K. Cho, *J. Phys. Chem. C*, 2009, **113**, 17579.
- 32 J. H. Kim, J. H. Park, J. H. Lee, J. S. Kim, M. Sim, C. Shim and K. Cho, *J. Mater. Chem.*, 2010, **20**, 7398.
- 33 G. H. Lu, L. G. Li, S. J. Li, Y. P. Qu, H. W. Tang and X. N. Yang, *Langmuir*, 2009, **25**, 3763.
- 34 D. J. Lipomi, R. C. Chiechi, M. D. Dickey and G. M. Whitesides, *Nano Lett.*, 2008, **8**, 2100.
- 35 S. P. Li, C. J. Newsome, D. M. Russell, T. Kugler, M. Ishida and T. Shimoda, *Appl. Phys. Lett.*, 2005, **87**, 062101.
- 36 S. Nagamatsu, W. Takashima, K. Kaneto, Y. Yoshida, N. Tanigaki and K. Yase, *Macromolecules*, 2003, **36**, 5252.
- 37 R. J. Kline, D. M. DeLongchamp, D. A. Fischer, E. K. Lin, L. J. Richter, M. L. Chabiny, M. F. Toney, M. Heeney and I. McCulloch, *Macromolecules*, 2007, **40**, 7960.
- 38 D. M. DeLongchamp, R. J. Kline, Y. Jung, D. S. Germack, E. K. Lin, A. J. Moad, L. J. Richter, M. F. Toney, M. Heeney and I. McCulloch, *ACS Nano*, 2009, **3**, 780.
- 39 H. N. Tsao, D. Cho, J. W. Andreasen, A. Rouhanipour, D. W. Breiby, W. Pisula and K. Mullen, *Adv. Mater.*, 2009, **21**, 209.
- 40 W. H. Lee, J. H. Cho and K. Cho, *J. Mater. Chem.*, 2010, **20**, 2549.
- 41 D. Li and Y. N. Xia, *Adv. Mater.*, 2004, **16**, 1151.
- 42 J. S. Stephens, D. B. Chase and J. F. Rabolt, *Macromolecules*, 2004, **37**, 877.
- 43 R. Jaeger, H. Schonherr and G. J. Vancso, *Macromolecules*, 1996, **29**, 7634.
- 44 D. O'Carroll, D. Iacopino, A. O'Riordan, P. Lovera, E. O'Connor, G. A. O'Brien and G. Redmond, *Adv. Mater.*, 2008, **20**, 42.
- 45 S. Moynihan, D. Iacopino, D. O'Carroll, P. Lovera and G. Redmond, *Chem. Mater.*, 2008, **20**, 996.
- 46 D. O'Carroll, I. Lieberwirth and G. Redmond, *Nat. Nanotechnol.*, 2007, **2**, 180.
- 47 E. C. Garnett, M. L. Brongersma, Y. Cui and M. D. McGehee, *Annu. Rev. Mater. Res.*, 2011, **41**, 269.
- 48 A. C. Mayer, S. R. Scully, B. E. Hardin, M. W. Rowell and M. D. McGehee, *Mater. Today*, 2007, **10**, 28.
- 49 E. Mena-Osteritz, A. Meyer and B. M. W. Langeveld-Voss, R. A. J. Janssen, E. W. Meijer and P. Bauerle, *Angew. Chem., Int. Ed.*, 2000, **39**, 2680.
- 50 P. Keg, A. Lohani, D. Fichou, Y. M. Lam, Y. L. Wu, B. S. Ong and S. G. Mhaisalkar, *Macromol. Rapid Commun.*, 2008, **29**, 1197.
- 51 W. H. Lee, J. Park, S. H. Sim, S. Lim, K. S. Kim, B. H. Hong and K. Cho, *J. Am. Chem. Soc.*, 2011, **133**, 4447.
- 52 G. Hlawacek, F. S. Khokhar, R. van Gastel, B. Poelsema and C. Teichert, *Nano Lett.*, 2011, **11**, 333.
- 53 M. Brinkmann and J. C. Wittmann, *Adv. Mater.*, 2006, **18**, 860.
- 54 L. H. Jimison, M. F. Toney, I. McCulloch, M. Heeney and A. Salleo, *Adv. Mater.*, 2009, **21**, 1568.
- 55 A. Babel, J. D. Wind and S. A. Jenekhe, *Adv. Funct. Mater.*, 2004, **14**, 891.
- 56 A. Babel, Y. Zhu, K. F. Cheng, W. C. Chen and S. A. Jenekhe, *Adv. Funct. Mater.*, 2007, **17**, 2542.
- 57 E. J. Meijer, D. M. De Leeuw, S. Setayesh, E. Van Veenendaal, B. H. Huisman, P. W. M. Blom, J. C. Hummelen, U. Scherf and T. M. Klapwijk, *Nat. Mater.*, 2003, **2**, 678.
- 58 A. Babel and S. A. Jenekhe, *Macromolecules*, 2004, **37**, 9835.
- 59 S. Goffri, C. Muller, N. Stingelin-Stutzmann, D. W. Breiby, C. P. Radano, J. W. Andreasen, R. Thompson, R. A. J. Janssen, M. M. Nielsen, P. Smith and H. Sirringhaus, *Nat. Mater.*, 2006, **5**, 950.

- 60 L. Qiu, J. A. Lim, X. Wang, W. H. Lee, M. Hwang and K. Cho, *Adv. Mater.*, 2008, **20**, 1141.
- 61 W. H. Lee, J. A. Lim, D. Kwak, J. H. Cho, H. S. Lee, H. H. Choi and K. Cho, *Adv. Mater.*, 2009, **21**, 4243.
- 62 L. L. Chua, P. K. H. Ho, H. Sirringhaus and R. H. Friend, *Adv. Mater.*, 2004, **16**, 1609.
- 63 A. C. Arias, F. Endicott and R. A. Street, *Adv. Mater.*, 2006, **18**, 2900.
- 64 A. Salleo and A. C. Arias, *Adv. Mater.*, 2007, **19**, 3540.
- 65 S. Walheim, M. Boltau, J. Mlynek, G. Krausch and U. Steiner, *Macromolecules*, 1997, **30**, 4995.
- 66 S. Y. Heriot and R. A. L. Jones, *Nat. Mater.*, 2005, **4**, 782.
- 67 T. Chatterjee, K. Yurekli, V. G. Hadjiev and R. Krishnamoorti, *Adv. Funct. Mater.*, 2005, **15**, 1832.
- 68 G. H. Lu, H. W. Tang, Y. P. Qu, L. G. Li and X. N. Yang, *Macromolecules*, 2007, **40**, 6579.
- 69 G. H. Lu, H. W. Tang, Y. A. Huan, S. J. Li, L. G. Li, Y. Z. Wang and X. N. Yang, *Adv. Funct. Mater.*, 2010, **20**, 1714.
- 70 L. Z. Qiu, W. H. Lee, X. H. Wang, J. S. Kim, J. A. Lim, D. Kwak, S. Lee and K. Cho, *Adv. Mater.*, 2009, **21**, 1349.
- 71 L. Z. Qiu, X. Wang, W. H. Lee, J. A. Lim, J. S. Kim, D. Kwak and K. Cho, *Chem. Mater.*, 2009, **21**, 4380.
- 72 J. A. Lim, W. H. Lee, H. S. Lee, J. H. Lee, Y. D. Park and K. Cho, *Adv. Funct. Mater.*, 2008, **18**, 229.
- 73 M. Singh, H. M. Haverinen, P. Dhagat and G. E. Jabbour, *Adv. Mater.*, 2010, **22**, 673.
- 74 H. Sirringhaus, T. Kawase, R. H. Friend, T. Shimoda, M. Inbasekaran, W. Wu and E. P. Woo, *Science*, 2000, **290**, 2123.
- 75 J. A. Lim, J. H. Kim, L. Qiu, W. H. Lee, H. S. Lee, D. Kwak and K. Cho, *Adv. Funct. Mater.*, 2010, **20**, 3292.
- 76 S. Ogawa, T. Naijo, Y. Kimura, H. Ishii and M. Niwano, *Appl. Phys. Lett.*, 2005, **86**, 252104.
- 77 J. A. DeFranco, B. S. Schmidt, M. Lipson and G. G. Malliaras, *Org. Electron.*, 2006, **7**, 22.
- 78 L. Z. Qiu, Q. Xu, W. H. Lee, X. H. Wang, B. Kang, G. Lv and K. Cho, *J. Mater. Chem.*, 2011, **21**, 15637.
- 79 J. S. Liu, E. Sheina, T. Kowalewski and R. D. McCullough, *Angew. Chem., Int. Ed.*, 2002, **41**, 329.
- 80 X. Yu, K. Xiao, J. H. Chen, N. V. Lavrik, K. L. Hong, B. G. Sumpter and D. B. Geohegan, *ACS Nano*, 2011, **5**, 3559.
- 81 G. Sauve and R. D. McCullough, *Adv. Mater.*, 2007, **19**, 1822.
- 82 C. Muller, S. Goffri, D. W. Breiby, J. W. Andreasen, H. D. Chanzy, R. A. J. Janssen, M. M. Nielsen, C. P. Radano, H. Sirringhaus, P. Smith and N. Stingelin-Stutzmann, *Adv. Funct. Mater.*, 2007, **17**, 2674.
- 83 P. T. Wu, G. Q. Ren, F. S. Kim, C. X. Li, R. Mezzenga and S. A. Jenekhe, *J. Polym. Sci., Part A: Polym. Chem.*, 2010, **48**, 614.
- 84 A. Babel, D. Li, Y. N. Xia and S. A. Jenekhe, *Macromolecules*, 2005, **38**, 4705.
- 85 N. J. Pinto, A. T. Johnson, A. G. MacDiarmid, C. H. Mueller, N. Theofylaktos, D. C. Robinson and F. A. Miranda, *Appl. Phys. Lett.*, 2003, **83**, 4244.
- 86 H. Q. Liu, C. H. Reccius and H. G. Craighead, *Appl. Phys. Lett.*, 2005, **87**.
- 87 R. Gonzalez and N. J. Pinto, *Synth. Met.*, 2005, **151**, 275.
- 88 N. J. Pinto, K. V. Carrasquillo, C. M. Rodd and R. Agarwal, *Appl. Phys. Lett.*, 2009, **94**.
- 89 S. Lee, G. D. Moon and U. Jeong, *J. Mater. Chem.*, 2009, **19**, 743.
- 90 S. W. Lee, H. J. Lee, J. H. Choi, W. G. Koh, J. M. Myoung, J. H. Hur, J. J. Park, J. H. Cho and U. Jeong, *Nano Lett.*, 2010, **10**, 347.
- 91 J. Y. Chen, C. C. Kuo, C. S. Lai, W. C. Chen and H. L. Chen, *Macromolecules*, 2011, **44**, 2883.
- 92 S. R. Forrest, *Nature*, 2004, **428**, 911.
- 93 C. J. Brabec, N. S. Sariciftci and J. C. Hummelen, *Adv. Funct. Mater.*, 2001, **11**, 15.
- 94 Y. Y. Liang, Z. Xu, J. B. Xia, S. T. Tsai, Y. Wu, G. Li, C. Ray and L. P. Yu, *Adv. Mater.*, 2010, **22**, E135.
- 95 R. F. Service, *Science*, 2011, **332**, 293.
- 96 H. Y. Chen, J. H. Hou, S. Q. Zhang, Y. Y. Liang, G. W. Yang, Y. Yang, L. P. Yu, Y. Wu and G. Li, *Nat. Photonics*, 2009, **3**, 649.
- 97 S. B. Jo, J. H. Lee, M. Sim, M. Kim, J. H. Park, Y. S. Choi, Y. Kim, S. G. Ihn and K. Cho, *Adv. Energy Mater.*, 2011, **1**, 690.
- 98 M. C. Scharber, D. Wuhlbacher, M. Koppe, P. Denk, C. Waldauf, A. J. Heeger and C. L. Brabec, *Adv. Mater.*, 2006, **18**, 789.
- 99 S. H. Park, A. Roy, S. Beaupre, S. Cho, N. Coates, J. S. Moon, D. Moses, M. Leclerc, K. Lee and A. J. Heeger, *Nat. Photonics*, 2009, **3**, 297.
- 100 J. K. Lee, W. L. Ma, C. J. Brabec, J. Yuen, J. S. Moon, J. Y. Kim, K. Lee, G. C. Bazan and A. J. Heeger, *J. Am. Chem. Soc.*, 2008, **130**, 3619.
- 101 G. J. Zhao, Y. J. He and Y. F. Li, *Adv. Mater.*, 2010, **22**, 4355.
- 102 Y. J. He, H. Y. Chen, J. H. Hou and Y. F. Li, *J. Am. Chem. Soc.*, 2010, **132**, 1377.
- 103 C. J. Brabec, A. Cravino, D. Meissner, N. S. Sariciftci, T. Fromherz, M. T. Rispen, L. Sanchez and J. C. Hummelen, *Adv. Funct. Mater.*, 2001, **11**, 374.
- 104 Y. Vaynzof, D. Kabra, L. H. Zhao, L. L. Chua, U. Steiner and R. H. Friend, *ACS Nano*, 2011, **5**, 329.
- 105 V. D. Mihailetschi, H. X. Xie, B. de Boer, L. J. A. Koster and P. W. M. Blom, *Adv. Funct. Mater.*, 2006, **16**, 699.
- 106 G. Li, V. Shrotriya, J. S. Huang, Y. Yao, T. Moriarty, K. Emery and Y. Yang, *Nat. Mater.*, 2005, **4**, 864.
- 107 F. Padinger, R. S. Rittberger and N. S. Sariciftci, *Adv. Funct. Mater.*, 2003, **13**, 85.
- 108 C. R. McNeill, J. J. M. Halls, R. Wilson, G. L. Whiting, S. Berkebile, M. G. Ramsey, R. H. Friend and N. C. Greenham, *Adv. Funct. Mater.*, 2008, **18**, 2309.
- 109 Y. Yao, J. H. Hou, Z. Xu, G. Li and Y. Yang, *Adv. Funct. Mater.*, 2008, **18**, 1783.
- 110 J. Peet, J. Y. Kim, N. E. Coates, W. L. Ma, D. Moses, A. J. Heeger and G. C. Bazan, *Nat. Mater.*, 2007, **6**, 497.
- 111 H. Hoppe and N. S. Sariciftci, *J. Mater. Chem.*, 2006, **16**, 45.
- 112 S. Berson, R. De Bettignies, S. Bailly and S. Guillerez, *Adv. Funct. Mater.*, 2007, **17**, 1377.
- 113 A. H. Rice, R. Giridharagopal, S. X. Zheng, F. S. Ohuchi, D. S. Ginger and C. K. Luscombe, *ACS Nano*, 2011, **5**, 3132.
- 114 A. J. Moule and K. Meerholz, *Adv. Funct. Mater.*, 2009, **19**, 3028.
- 115 C. Muller, T. A. M. Ferenczi, M. Campoy-Quiles, J. M. Frost, D. D. C. Bradley, P. Smith, N. Stingelin-Stutzmann and J. Nelson, *Adv. Mater.*, 2008, **20**, 3510.
- 116 N. C. Cates, R. Gysel, Z. Beiley, C. E. Miller, M. F. Toney, M. Heeney, I. McCulloch and M. D. McGehee, *Nano Lett.*, 2009, **9**, 4153.
- 117 A. C. Mayer, M. F. Toney, S. R. Scully, J. Rivnay, C. J. Brabec, M. Scharber, M. Koppe, M. Heeney, I. McCulloch and M. D. McGehee, *Adv. Funct. Mater.*, 2009, **19**, 1173.
- 118 J. Smith, R. Hamilton, I. McCulloch, N. Stingelin-Stutzmann, M. Heeney, D. D. C. Bradley and T. D. Anthopoulos, *J. Mater. Chem.*, 2010, **20**, 2562.
- 119 R. A. L. Jones, L. J. Norton, E. J. Kramer, F. S. Bates and P. Wiltzius, *Phys. Rev. Lett.*, 1991, **66**, 1326.
- 120 J. S. Kim, Y. Lee, J. H. Lee, J. H. Park, J. K. Kim and K. Cho, *Adv. Mater.*, 2010, **22**, 1355.
- 121 H. Xin, F. S. Kim and S. A. Jenekhe, *J. Am. Chem. Soc.*, 2008, **130**, 5424.
- 122 P. T. Wu, H. Xin, F. S. Kim, G. Q. Ren and S. A. Jenekhe, *Macromolecules*, 2009, **42**, 8817.
- 123 B. G. Kim, M. S. Kim and J. Kim, *ACS Nano*, 2010, **4**, 2160.
- 124 C. Piliago, T. W. Holcombe, J. D. Douglas, C. H. Woo, P. M. Beaujuge and J. M. J. Frechet, *J. Am. Chem. Soc.*, 2010, **132**, 7595.
- 125 J. S. Moon, C. J. Takacs, S. Cho, R. C. Coffin, H. Kim, G. C. Bazan and A. J. Heeger, *Nano Lett.*, 2010, **10**, 4005.
- 126 A. Gadisa, W. D. Oosterbaan, K. Vandewal, J. C. Bolese, S. Bertho, J. D'Haen, L. Lutsen, D. Vanderzande and J. V. Manca, *Adv. Funct. Mater.*, 2009, **19**, 3300.
- 127 L. H. Nguyen, H. Hoppe, T. Erb, S. Gunes, G. Gobsch and N. S. Sariciftci, *Adv. Funct. Mater.*, 2007, **17**, 1071.
- 128 Z. Y. Wu, A. Petzold, T. Henze, T. Thurn-Albrecht, R. H. Lohwasser, M. Sommer and M. Thelakkat, *Macromolecules*, 2010, **43**, 4646.
- 129 W. Ma, J. Y. Kim, K. Lee and A. J. Heeger, *Macromol. Rapid Commun.*, 2007, **28**, 1776.
- 130 C. H. Woo, B. C. Thompson, B. J. Kim, M. F. Toney and J. M. J. Frechet, *J. Am. Chem. Soc.*, 2008, **130**, 16324.
- 131 R. J. Kline, M. D. McGehee, E. N. Kadnikova, J. S. Liu and J. M. J. Frechet, *Adv. Mater.*, 2003, **15**, 1519.
- 132 Y. D. Park, D. H. Kim, Y. Jang, J. H. Cho, M. Hwang, H. S. Lee, J. A. Lim and K. Cho, *Org. Electron.*, 2006, **7**, 514.

- 133 W. D. Oosterbaan, V. Vrindts, S. Berson, S. Guillerez, O. Douheret, B. Ruttens, J. D'Haen, P. Adriaensens, J. Manca, L. Lutsen and D. Vanderzande, *J. Mater. Chem.*, 2009, **19**, 5424.
- 134 J. S. Kim, Y. Park, D. Y. Lee, J. H. Lee, J. H. Park, J. K. Kim and K. Cho, *Adv. Funct. Mater.*, 2010, **20**, 540.
- 135 C.-Y. Chang, C.-E. Wu, S.-Y. Chen, C. Cui, Y.-J. Cheng, C.-S. Hsu, Y.-L. Wang and Y. Li, *Angew. Chem., Int. Ed.*, 2011, **50**, 9386.
- 136 A. L. Briseno, T. W. Holcombe, A. I. Boukai, E. C. Garnett, S. W. Shelton, J. J. M. Frechet and P. D. Yang, *Nano Lett.*, 2010, **10**, 334.
- 137 S. Q. Ren, N. Zhao, S. C. Crawford, M. Tambe, V. Bulovic and S. Gradecak, *Nano Lett.*, 2011, **11**, 408.
- 138 S. Q. Ren, L. Y. Chang, S. K. Lim, J. Zhao, M. Smith, N. Zhao, V. Bulovic, M. Bawendi and S. Gradecak, *Nano Lett.*, 2011, **11**, 3998.
- 139 C. Y. Kuo, W. C. Tang, C. Gau, T. F. Guo and D. Z. Jeng, *Appl. Phys. Lett.*, 2008, 93.
- 140 J. Ackermann, C. Videlot, A. El Kassmi, R. Guglielmetti and F. Fages, *Adv. Funct. Mater.*, 2005, **15**, 810.
- 141 M. Hirade, H. Nakanotani, M. Yahiro and C. Adachi, *ACS Appl. Mater. Interfaces*, 2011, **3**, 80.
- 142 A. I. Hochbaum and P. D. Yang, *Chem. Rev.*, 2010, **110**, 527.
- 143 M. Aryal, K. Trivedi and W. C. Hu, *ACS Nano*, 2009, **3**, 3085.
- 144 K. Kim, J. W. Lee, S. H. Lee, Y. B. Lee, E. H. Cho, H. S. Noh, S. G. Jo and J. Joo, *Org. Electron.*, 2011, **12**, 1695.
- 145 M. R. Lee, R. D. Eckert, K. Forberich, G. Dennler, C. J. Brabec and R. A. Gaudiana, *Science*, 2009, **324**, 232.